The Extracellular ATP Receptor P2RX7 Imprints a Promemory Transcriptional Signature in Effector CD8$^+$ T Cells

Trupti Vardam-Kaur,*[,1] Sarah van Dijk,*[,1] Changwei Peng,[†] Kelsey M. Wanhainen,[†] Stephen C. Jameson,[†] and Henrique Borges da Silva*

Development of CD8$^+$ central memory T (Tcm) and resident memory T (Trm) cells, which promote immunity in the circulation and in barrier tissues, respectively, is not completely understood. Tcm and Trm cells may arise from common precursors; however, their fate-inducing signals are elusive. We found that virus-specific effector CD8$^+$ T cells display heterogeneous expression of the extracellular ATP sensor P2RX7. P2RX7-high expression is confined, at peak effector phase, to CD62L$^+$ memory precursors, which preferentially form Tcm cells. Among early effector CD8$^+$ T cells, asymmetrical P2RX7 distribution correlated with distinct transcriptional signatures, with P2RX7-high cells enriched for memory and tissue residency sets. P2RX7-high early effectors preferentially form both Tcm and Trm cells. Defective Tcm and Trm cell formation in P2RX7 deficiency is significantly reverted when the transcriptional repressor Zeb2 is ablated. Mechanistically, P2RX7 negatively regulates Zeb2 expression, at least partially through TGF-β sensing in early effector CD8$^+$ T cells. Our study indicates that unequal P2RX7 upregulation in effector CD8$^+$ T cells is a foundational element of the early Tcm/Trm fate. ***The Journal of Immunology*****, 2022, 208: 1686–1699.**

The development of immunological memory is paramount for host protection against secondary pathogen exposure (1). The establishment of Ag-specific cytotoxic memory CD8$^+$ T cells is specifically important for antiviral protective immunity (2). Over the past two decades, it has become clear that CD8$^+$ T cell memory is composed of distinct cell subsets with different migration, function, and longevity properties (3). These characteristics revealed four major memory CD8$^+$ T cell subsets. Long-lived effector cells (LLECs) are mostly confined to blood and blood-associated tissues (4, 5), whereas effector memory cells (Tem) recirculate between secondary lymphoid organs, blood, and nonlymphoid tissues (4). Two other subsets display heightened longevity, secondary response potential, and stemness: central memory T (Tcm) cells, which are mostly present in secondary lymphoid organs and express the defining marker L-selectin (CD62L) (6), and tissue resident memory T (Trm) cells, which are prominent in nonlymphoid tissues and, in normal circumstances, do not recirculate (7–9). Tcm and Trm cells, although present in distinct environments, share many transcriptional and functional characteristics (10) and may arise from common precursors (11). Previous studies suggest that these common precursors are found at the early effector immune response and express low levels of the terminal effector (TE)-linked molecule killer cell lectin-like receptor subfamily G member 1 (KLRG1) and high levels of the stemness-associated transcription factor T cell factor 1 (TCF-1) (12–16). Although considerable advances have been made in the transcriptional and metabolic control of early memory precursors (MPs) (13–18), less is known about whether and how extracellular signals contribute to early diversion toward the memory fate. Understanding how this occurs will help identify factors simultaneously promoting Tcm and Trm cells.

Many extracellular signals can be sensed by Ag-specific CD8$^+$ T cells, such as cytokines (e.g., IL-7, IL-2, IL-15, IFN-γ) and chemokines (e.g., CXCL9, CXCL10) that are mostly produced by APCs or stromal cells (4, 19–21). Other signals can be released passively by the inflamed tissue or infected cells, such as nucleotides (e.g., ATP) (22). Extracellular ATP (eATP) can be sensed by CD8$^+$ T cells through the low-affinity ion channel P2RX7 (23). In recent studies, we have defined that CD8-intrinsic P2RX7 is required for the establishment of both Tcm and Trm cells (24, 25). P2RX7 promotes metabolic adaptations fundamental for memory CD8$^+$ T cell differentiation, namely activation of the AMP kinase signaling pathway and promotion of mitochondrial function (24). We have also found that P2RX7 promotes the upregulation of the TGF-β signaling pathway (25), which is crucial for epithelial Trm populations (26). Both Tcm and Trm cells express high levels of and require P2RX7, suggesting two possible scenarios for how P2RX7 simultaneously promotes these subsets. First, P2RX7 stimulation may promote survival of Tcm and Trm cells after they have differentiated,

*Department of Immunology, Mayo Clinic Arizona, Scottsdale, AZ; and [†]Center for Immunology, Department of Laboratory Medicine and Pathology, University of Minnesota, Minneapolis, MN

[1]T.V.-K. and S.v.D. contributed equally to this work.

ORCIDs: 0000-0003-1458-1902 (T.V.-K.); 0000-0002-7832-561X (S.v.D.); 0000-0002-0710-9573 (C.P.); 0000-0001-9137-1146 (S.C.J.); 0000-0001-9424-3326 (H.B.d.S.).

Received for publication June 10, 2021. Accepted for publication January 25, 2022.

This work was supported by National Institute of Allergy and Infectious Diseases grants awarded to H.B.d.S. (R00 AI139381) and to S.C.J. (R01 AI038903, AI145147).

H.B.d.S. conceived the project and designed the experiments. H.B.d.S. and S.C.J. provided mice and reagents for all experiments. T.V.-K., S.v.D., C.P., K.M.W., and H.B.d.S. performed the experiments. T.V.-K., S.v.D. and H.B.d.S. analyzed the data. H.B.d.S. wrote the manuscript with input from all authors.

Address correspondence and reprint requests to Henrique Borges da Silva, Mayo Clinic, 13400 E. Shea Boulevard, Samuel C. Johnson Building 3-364, Scottsdale, AZ 85259. E-mail address: borgesdasilva.henrique@mayo.edu

The online version of this article contains supplemental material.

Abbreviations used in this article: DEG, differentially expressed gene; eATP, extracellular ATP; GSEA, gene set enrichment analysis; GzmB, granzyme B; KLRG1, killer cell lectin-like receptor subfamily G member 1; KO, knockout; LCMV, lymphocytic choriomeningitis virus; LCMV-Arm, lymphocytic choriomeningitis virus Armstrong; LLEC, long-lived effector cell; MP, memory precursor; MTG, MitoTracker Green; RNA-seq, RNA sequencing; RNP, ribonucleoprotein; RV-EV, empty virus retroviral vector; SG, salivary gland; SI IEL, small intestine intraepithelial lymphocyte; TCF-1, T cell factor 1; Tcm, central memory T; TE, terminal effector; Tem, effector memory T; TMRE, tetramethylrhodamine ethyl ester; Trm, resident memory T; WT, wild type.

sustaining each subset independently. Our previous results suggest that this is at least partially the case, because continued P2RX7 expression is needed for Tcm and Trm maintenance (25). Alternatively, intracellular pathways affected by P2RX7 may be induced in early effector $CD8^+$ T cells with the potential to become either Tcm or Trm cells; that is, P2RX7 signaling could promote the arising of early MPs. Indeed, the role of P2RX7 in upregulation of the TGF-β signaling pathway occurs at the early effector phase (25).

In this study, we report that P2RX7 simultaneously promotes establishment of Tcm and Trm cells through positive control of a subset of early MPs. We show that P2RX7 expression at the early effector phase is not homogeneous and that early effector $CD8^+$ T cells expressing higher levels of P2RX7 preferentially form long-lived Tcm and Trm populations. Performing a transcriptional comparison between P2RX7 high- versus low-expressing early effector $CD8^+$ T cells, we find that many promemory and proresidency gene signatures are enriched in P2RX7-expressing early effector $CD8^+$ T cells. Finally, we provide evidence that P2RX7-mediated downregulation of the transcriptional repressor Zeb2 aids in the acquisition of an early MP phenotype and subsequent Tcm and Trm cell establishment. These results indicate that the eATP receptor P2RX7 plays a crucial role in the initial differentiation of Tcm/Trm common MPs, serving as an important extracellular environment sensor inducing a memory fate in effector $CD8^+$ T cells.

Materials and Methods

Mice

Female C57BL/6 (B6) and B6.SJL (expressing the CD45.1 allele) mice were purchased from the National Cancer Institute (via Charles River; catalog nos. 556 and 564, respectively). *P2rx7*$^{-/-}$ (catalog no. 005576) and CD4-Cre (catalog no. 022071) mice were obtained from The Jackson Laboratory and were both fully backcrossed onto a C57BL/6 background. *P2rx7*$^{fl/fl}$ mice were obtained from Drs. Gyorgy Hasko (Rutgers University) and Matyas Sandor (University of Wisconsin), and they were crossed onto the C57BL/6 background and with CD4-Cre mice. Lymphocytic choriomeningitis virus (LCMV)-D^bGP33-specific TCR transgenic P14 mice were fully backcrossed to B6, *P2rx7*$^{-/-}$, CD4-Cre, and CD4-Cre *P2rx7*$^{fl/fl}$ mice, with introduction of CD45.1 and CD45.2 congenic markers for identification. Animals were maintained under specific pathogen-free conditions at the University of Minnesota and at Mayo Clinic Arizona. In all experiments, mice were randomly assigned to experimental groups. All experimental procedures were approved by the institutional animal care and use committee at the University of Minnesota (IACUC 1709-35136A) or at Mayo Clinic Arizona (IACUC A00005542-20).

Viral strains

The LCMV Armstrong (LCMV-Arm) strain was maintained at −80°C until infection and diluted to 2×10^6 PFU/ml in PBS.

Infection studies

Wild-type (WT), *P2rx7*$^{-/-}$, or CD4-Cre *P2rx7*$^{fl/fl}$ P14 cells were adoptively transferred into naive WT mice, which were infected with the LCMV-Arm strain (2×10^5 PFU, i.p.).

Primary cell cultures

Naive P14 cells were obtained from 6- to 8-wk-old male or female mice with a C57BL/6 background. When appropriate, naive P14 cells were activated for 72 h in the presence of anti-CD3ε (10 μg/ml) + anti-CD28 (20 μg/ml) + mouse recombinant IL-2 (10 ng/ml) diluted in complete RPMI media: RPMI 1640 (Corning) supplemented with 10% FBS (Atlanta Biologicals), 100 U/ml penicillin/streptomycin (Thermo Fisher Scientific), and 2 mM L-glutamine (Corning). In other experiments, effector P14 cells were cultured for 40 h in the presence of recombinant TGF-β (10 ng/ml). All cells were cultured at 37°C in a humidified atmosphere containing 5% CO_2.

Adoptive cell transfer

$CD8^+$ P14 cells were negatively enriched (using the $CD8^+$ T cell isolation kit; Miltenyi Biotec) from WT ($CD45.1/2^+$) and *P2rx7*$^{-/-}$ ($CD45.2/2^+$) P14 mice. The cell populations were mixed at a ratio of 1:1, and a total of 5×10^4 P14 cells were coadoptively transferred into recipient mice ($CD45.1/1^+$), which were infected the next day with LCMV-Arm. At appropriated times after infection, mice were sacrificed for analysis. In other experiments, WT ($CD45.2/2^+$) or CD4-Cre *P2rx7*$^{fl/fl}$ ($CD45.2/2^+$) P14 cells were negatively enriched and individually adoptively transferred (5×10^4 cells) into recipient mice ($CD45.1/1^+$), which were infected with LCMV-Arm.

For the secondary adoptive transfer experiments, $CD45.2/2^+$ $P2RX7^{hi}$ or $P2RX7^{lo}$ MPs or day 4.5 effector P14 cells were sorted from the spleens of recipient mice, then adoptively transferred (3×10^5 cells) into infection-matched recipient mice ($CD45.1/1^+$). At the appropriate time points after transfer, mice were sacrificed for analysis.

Flow cytometry

Lymphocytes were isolated from tissues, including spleen, blood, small intestine epithelium (small intestine intraepithelial lymphocytes [SI IELs]), liver, and salivary glands (SGs) as previously described (27, 28). In summary, organs were removed, cut into small pieces, and placed into Erlenmeyer flasks containing 30 ml of 0.5 mg/ml collagenase type I solution (SGs) or 0.15 mg/ml DTT (SI IELs). After this period, lymphocytes were isolated by 44/67% Percoll gradient isolation. During isolation of lymphocytes from nonlymphoid tissues, in all experiments, 50 μg of Treg-Protector (anti-ARTC2.2) nanobodies (BioLegend) were injected i.v. 30 min before mouse sacrifice (29). Direct ex vivo staining and intracellular staining were performed as described (27, 30). To identify LCMV-specific $CD8^+$ T cells, PE- or allophycocyanin-gp33-41 tetramers were obtained from the National Institutes of Health Tetramer Core. For detection of vascular-associated lymphocytes in nonlymphoid organs, in vivo i.v. injection of PerCP-cyanine 5.5–conjugated CD8α Ab was performed (31). Due to unclear division between bona fide Trm cells and circulating memory cells using i.v. CD8α injection in the liver, we used total liver P14 numbers in all experiments where this organ is listed. Among LCMV-specific $CD8^+$ T cells, the following markers were used to distinguish these respective populations: Tcm ($CD44^+CD62L^+$), Tem ($CD44^+CD62L^-CD127^+$), LLEC ($CD44^+CD62L^-CD127^-KLRG1^{hi}$), Trm (i.v.$CD8\alpha^-CD69^{+/-}CD103^{hi/int/lo}$), MPs ($CD127^+KLRG1^-$), and TEs ($CD127^-KLRG1^+$). Other surface Abs used were as follows: CD25, CD103, P2RX7, CXCR5, Tim3, PD1, CD101, and integrin β7 (all Abs from BioLegend). For detection of the intracellular factor TCF-1, surface-stained cells were permeabilized, fixed, and stained by using the eBioscience Foxp3 staining kit according to the manufacturer's instructions. For detection of cytokine production, spleen cells or cell-sorted P14 cells were stimulated in vitro with PMA + ionomycin (eBioscience Cell Stimulation Cocktail) in the presence of monensin (GolgiStop; BD Biosciences). After 4 h, cells were stained with extracellular Abs, then fixed and stained with intracellular Abs for IFN-γ (BioLegend) and granzyme B (GzmB) (BD Biosciences). Mitochondrial mass and membrane potential were assessed using staining with the fluorescent dyes MitoTracker Green (MTG; Thermo Fisher Scientific) and tetramethylrhodamine ethyl ester (TMRE; BD Biosciences) as described before (24). Flow cytometric analysis was performed on an LSR II or LSR Fortessa device (BD Biosciences), and data were analyzed using FlowJo software (BD Biosciences).

Cell sorting

Cell sorting was performed on a FACSAria III device (BD Biosciences). RNA expression experiments were performed with $CD45.1/2^+$ WT ($CD44^+$) and $CD45.2/2^+$ *P2rx7*$^{-/-}$ ($CD44^+$) P14 $CD8^+$ T cells sorted from mice 4.5 d after LCMV infection or with $CD45.2/2^+$ $P2RX7^{hi}CD44^+$ and $CD45.2/2^+$ $P2RX7^{lo}CD44^+$ P14 $CD8^+$ T cells from mice 4.5 d after LCMV infection. Secondary adoptive transfer experiments were done with $P2RX7^{hi}$ and $P2RX7^{lo}$ $KLRG1^-CD127^+$ (MPs) P14 $CD8^+$ T cells from mice 8 d after LCMV infection, with $CD62L^+CD44^+$ (Tcm) P14 $CD8^+$ T cells from mice 30 d after LCMV infection, or with $P2RX7^{hi}CD44^+$ and $P2RX7^{lo}CD44^+$ P14 $CD8^+$ T cells from mice 4.5 d after LCMV infection. The population purity after cell sorting was >95% in all experiments.

RNA-sequencing and bioinformatics analysis

WT or *P2rx7*$^{-/-}$ P14 cells sorted from spleens at day 4.5 after LCMV infection were first homogenized using QIAshredder columns (Qiagen), and RNA was extracted using the RNeasy Plus Mini Kit (Qiagen) following the manufacturer's instructions. Library preparation and RNA sequencing (RNA-seq) libraries were prepared, and RNA-seq (150-bp paired-end reads, NovaSeq 6000; Illumina) was done at the University of Minnesota Genomics Center. RNA-seq reads were mapped and counted by collection of hierarchical UMII-RIS pipelines to generate the raw count matrix. The raw count values were converted to fragments per kilobase million values and were further transformed to z-score values to perform principal component analysis. Differentially expressed gene (DEG) analysis was done using DESeq2 (32). Genes with more than twofold changes and false discovery rate <0.05 were kept for gene cluster analysis.

P2RX7^{hi} or P2RX7^{lo} P14 cells sorted from spleens at day 4.5 after LCMV infection were homogenized using QIAshredder, and RNA was extracted using the RNeasy Plus Mini Kit as described before. Library preparation and RNA-seq (DNBseq platform, PE 100-bp paired-end read length) was done by BGI Americas. RNA-seq reads were mapped, and raw count matrix was generated. DEG analysis was done using DESeq2, and genes with greater than twofold changes and false discovery rate <0.05 were considered for gene cluster analysis.

Heatmaps were generated using the Morpheus software (Broad Institute; https://software.broadinstitute.org/morpheus/). RStudio was used to generate volcano plots of DEGs. Gene set enrichment analysis (GSEA) software was used to generate comparisons with gene sets from previous studies (summarized in Supplemental Table I). For the P2RX7^{hi} versus P2RX7^{lo} analysis, BGI provided customized analysis of DEGs, principal component analysis plots, and GSEA between groups.

CRISPR-Cas9 experiments

Cas9/ribonucleoprotein (RNP) nucleofection of P14 cells was performed as described previously (33). Briefly, P14 cells were isolated and activated as described above. While cells were maintained in culture, single-guide RNAs for *Zeb2* or *Cd4* and Cas9 protein were mixed by pipetting up and down and precomplexed at room temperature for at least 10 min. After this period, 1 million to 10 million activated P14 cells were resuspended in 20 μl of primary cell nucleofection solution (Lonza), then mixed and incubated with the crRNA/Cas9 mix for 2 min at room temperature. The P14 cell–Cas9–RNP mixes were transferred to nucleofection cuvette strips (4D-Nucleofector X kit S; Lonza). Cells were electroporated using a 4D nucleofector (4D-Nucleofector Core Unit; Lonza). After nucleofection, prewarmed complete RPMI was used to transfer transfected P14 cells in 96-well plates. After 2 h, P14 cells were cultured in 24-well plates in complete RPMI (+ IL-2 at 10 ng/ml) for 48 h before adoptive transfer into recipient mice (1×10^5 cells/mouse). Knockout (KO) efficiency was assessed using Sanger-based sequencing (GENEWIZ/Azenta Life Sciences), followed by analysis using the Inference of CRISPR Edits platform (Synthego). The single-guide RNAs used were *Cd4*_1: 5′-UCUUCCCUUGAGUGACAGCU-3′; *Cd4*_2: 5′-CAACUCCUAGCUGUCACUCA-3′; *Zeb2*_1: 5′-CCUGGUCCAGAGGGUUUGCA-3′; *Zeb2*_2: 5′-GGUGAACUAUGACAACGUAG-3′.

Retroviral transduction of P14 cells

Control empty retroviral vectors (empty virus or RV-EV) and *Tgfbr2*-encoding vectors (RV-*Tgfbr2*) were collected as supernatants of Plat-E–infected cells. In vitro activated P14 cells (after 24 h of activation) were transduced via spinfection with RV-EV or RV-*Tgfbr2* supernatants, as previously described (25). Cells were rested in the presence of IL-2 for an additional 48 h before further experiments.

Quantification and statistical analysis

Details on statistics used can be found in the figure legends. Data were subjected to the Kolmogorov-Smirnov test to assess the normality of samples. Statistical differences were calculated by using unpaired two-tailed Student *t* test (or one-way ANOVA with Tukey posttest, where indicated). All experiments were analyzed using Prism 7 (GraphPad Software). Graphical data were shown as mean values with error bars indicating the SD. The *p* values <0.05 (*), <0.01 (**), <0.001 (***), or <0.0001 (****) indicated significant differences between groups. A list of all *p* values can be found in Supplemental Table I.

Results

P2RX7 expression is heterogeneous within CD8$^+$ MPs and correlates with promemory molecules

In recent studies, we have found that in response to systemic viral infections such as LCMV, P2RX7 is quickly upregulated in effector CD8$^+$ T cells (25). At peak effector phase, P2RX7 is preferentially expressed by MP CD8$^+$ T cells compared with TEs (24) (Fig. 1A). The expression pattern of P2RX7 within MPs, however, is not homogeneous, being found instead as a continuum (Fig. 1B). An arbitrary division between MPs expressing the highest P2RX7 (P2RX7^{hi}) and the lowest P2RX7 (P2RX7^{lo}) revealed profound differences in their phenotypes. CD62L expression marks Tcm precursors (13) in ∼2% of Ag-specific CD8$^+$ T cells. CD62L expression is preferentially found in MPs (Supplemental Fig. 1A), almost exclusively confined to P2RX7^{hi} MPs (Fig. 1B). In addition, the expression of many other proteins preferentially expressed by memory CD8$^+$ T cells is higher in P2RX7^{hi} MPs, such as CD44, CD101, TCF-1 (Fig. 1C, 1D), CXCR5 (Supplemental Fig. 1B), and even the MP-defining molecule CD127 (Supplemental Fig. 1C). CD44 is also preferentially expressed in the few (<2%; data not shown) P2RX7^{hi} TEs (Fig. 1C, 1D). Expression of CD8α itself is also preferentially found in P2RX7^{hi} MPs, although the same pattern can also be seen when TEs are divided into P2RX7^{hi} and P2RX7^{lo} groups (Supplemental Fig. 1D). Conversely, expression of the exhaustion/TE marker Tim3 is preferentially found in P2RX7^{lo} MPs (Fig. 1C, 1D). All of these expression patterns are also true when adoptively transferred, LCMV-specific P14 cells are assessed (Supplemental Fig. 1E). P2RX7^{hi} P14 MPs also display decreased production of the effector cytokine IFN-γ when compared with P2RX7^{lo} counterparts or P14 TEs (Fig. 1E, 1F). GzmB production, in contrast, is unaltered (Fig. 1E, 1F). Overall, our data show that the MP subset displays significant phenotypic heterogeneity, which can be defined by P2RX7 expression level.

High P2RX7 expression in MPs favors differentiation of Tcm cells

The heterogeneity found within MPs suggested that P2RX7 expression levels may correlate with differentiation into long-lived memory T cells. To assess this, we sorted P2RX7^{hi} and P2RX7^{lo} MP P14 cells and performed secondary transfers into infection-matched mice (Fig. 1G). As positive controls, we sorted and adoptively transferred Tcm P14 cells, which were efficiently maintained in recipient mice upon secondary transfer (Fig. 1G, 1H) (34). Within the MP pool, P2RX7^{hi} cells were present in significantly higher numbers than P2RX7^{lo} counterparts (Fig. 1G, 1H) and displayed an increased proportion of CD62L-expressing cells (i.e., a Tcm phenotype) (Fig. 1H). The expression of P2RX7 remained higher in P2RX7^{hi} MP progenies (Fig. 1H), but even within the fewer P2RX7^{lo} MP progenies, we found increased P2RX7 expression compared with initial expression levels on donor cells (Fig. 1H). Overall, these data indicate that higher P2RX7 expression in MPs favors the establishment of memory CD8$^+$ T cells, especially the Tcm subset.

Qualitative and quantitative differences in P2RX7 expression correlate with a promemory transcriptional and protein signature in early effector CD8$^+$ T cells

Our findings within the MP subset strongly suggest that heterogeneity in P2RX7 expression helps define CD8$^+$ T cells that preferentially establish memory subsets. However, Trm cells do not exclusively arise from MPs; rather, they are derived from precursors found in the circulation at the early effector phase (35). P2RX7 expression is also heterogeneous in spleen early effector CD8$^+$ T cells (Fig. 2A); thus, we hypothesized that P2RX7 levels would also correlate with the expression of promemory markers. First, we conducted a transcriptional assessment of whether the presence of P2RX7 in early effectors would be associated with a promemory signature. RNA-seq analysis of WT versus *P2rx7*$^{-/-}$ early effector P14 cells revealed >200 DEGs (Fig. 2B, 2C, Supplemental Table I). WT P14 early effectors are enriched for many genes usually found in memory CD8$^+$ T cells, such as *Cd101*, *Bach2*, *Ccr7*, *Cxcr5*, and *Tcf7* (13, 16, 36) (Fig. 2C, Supplemental Table I). Simultaneously, genes preferentially associated with a Trm phenotype, such as *Itgae* (37), are enriched in WT early effectors (Fig. 2C, Supplemental Table I). Conversely, *P2rx7*$^{-/-}$ early effectors are enriched for either TE-linked genes (e.g., *Cx3cr1*, *Klrg1*, *Zeb2*) (13, 16, 36) or genes typically downregulated in Trm cells, such as *S1pr1* and *S1pr5* (27, 37) (Fig. 2C, Supplemental Table I). Predictably, many pathways associated with memory CD8$^+$ T cells, such as stemness related, are enriched in WT early effectors (Supplemental Table I). Simultaneously, apoptosis-related pathways

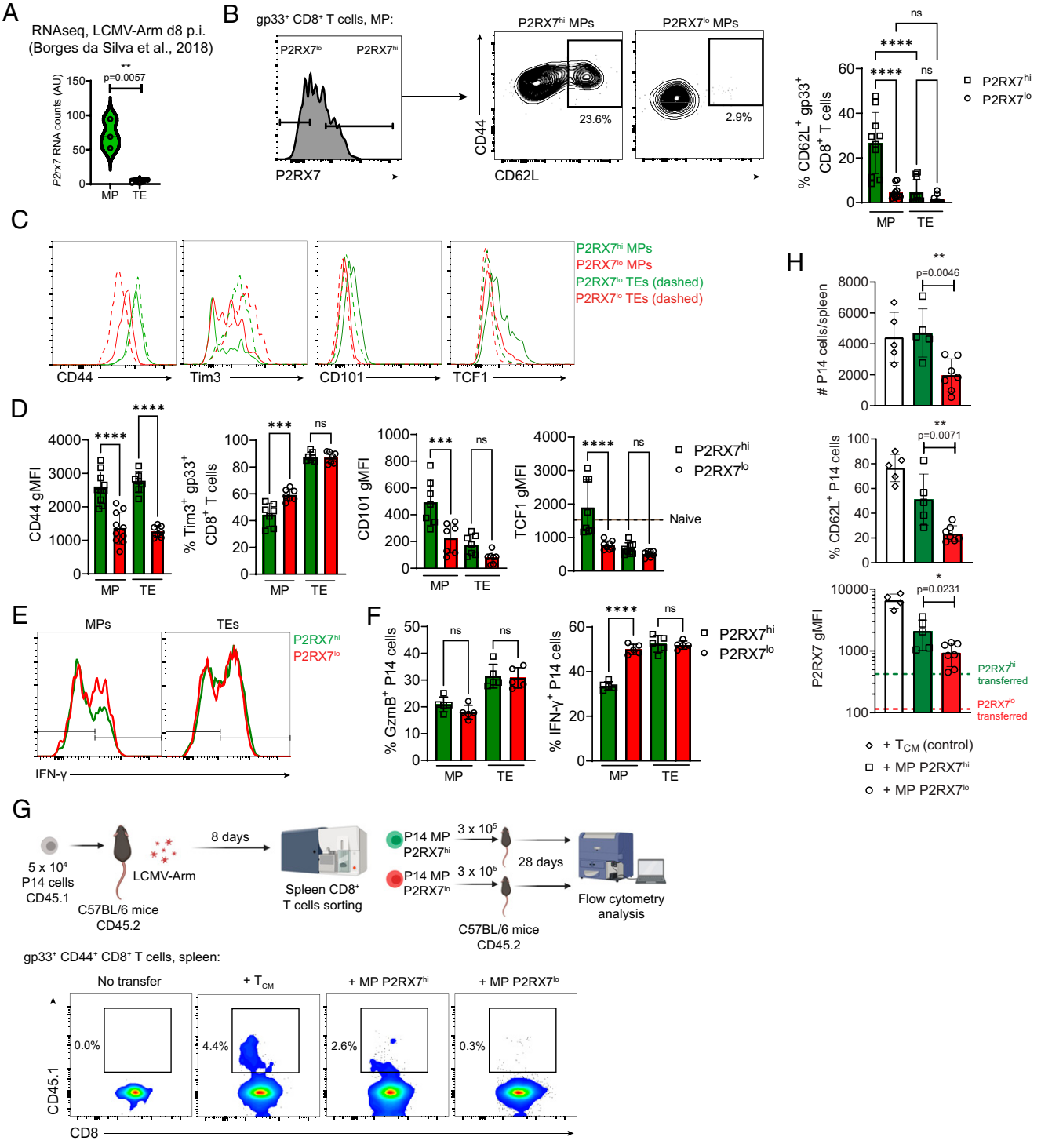

FIGURE 1. P2RX7 expression is heterogeneous among MPs and favors Tcm generation. (**A**) *P2rx7* mRNA counts from an RNA-seq comparison between MPs and TEs done by our group in a previous study. (**B–D**) C57BL/6 mice were infected with LCMV-Arm and harvested at 8 d after infection (p.i.). The protein expression of multiple molecules in Ag-specific (gp33-tetramer$^+$) CD8$^+$ MPs is shown. (B) Left: representative histogram showing P2RX7 expression in gp33$^+$ MPs. Center: Representative contour plots showing the expression of CD44 and CD62L in P2RX7^{hi} versus P2RX7^{lo} MPs. Right: Average percentages of CD62L$^+$ cells within P2RX7^{hi} (green, open squares) and P2RX7^{lo} (red, open circles) MPs and TEs. (C) Representative histograms of the expression of CD44, Tim3, CD101, and TCF1 in P2RX7^{hi} (green) and P2RX7^{lo} (red) MPs (solid lines) and TEs (dashed lines). (D) Geometric mean fluorescence intensity (gMFI) average values of CD44, CD101, and TCF-1 and percentages of Tim3$^+$ in P2RX7^{hi} (green, open squares) and P2RX7^{lo} (red, open circles) MPs and TEs. (**E** and **F**) In some experiments, P2RX7^{hi} (30% highest) and P2RX7^{lo} (30% lowest) MPs and TEs were cell sorted and reactivated in vitro with PMA and ionomycin. (E) Representative histograms showing production of IFN-γ in P2RX7^{hi} versus P2RX7^{lo} P14 MPs and TEs. (F) Average percentages of GzmB$^+$ (left) and IFN-γ$^+$ P2RX7^{hi} versus P2RX7^{lo} P14 MPs and TEs. (**G**) P14 cells (CD45.1$^+$) were transferred to C57BL/6 (CD45.2$^+$) mice, which were subsequently infected with LCMV-Arm. After 8 d, P2RX7^{hi} P14 MPs (30% highest) and P2RX7^{lo} P14 MPs (30% lowest) were sorted and adoptively transferred into infection-matched C57BL/6 mice (3×10^5 cells/mouse). After 28 d, the numbers and phenotype of transferred P14 cells were assessed in spleens of recipient mice using flow cytometry. On the bottom, representative plots showing the P14 populations present in recipient mice, including negative (No transfer) and positive (+ Tcm) controls. (**H**) Numbers of transferred P14 cells/spleen (top left), percentage of CD62L$^+$ P14 cells (bottom left), and P2RX7 gMFI (top right) in recipient mice for positive control (Tcm) cells (white, open diamonds), P2RX7^{hi} MPs (green, open squares), and P2RX7^{lo} MPs (red, open circles). (A, B, D, F, H) One-way ANOVA, $*p < 0.05$, $**p < 0.01$, $***p < 0.001$, $****p < 0.0001$. (B–F) Average values ± SD; data pooled from three independent experiments ($n = 4–10$).

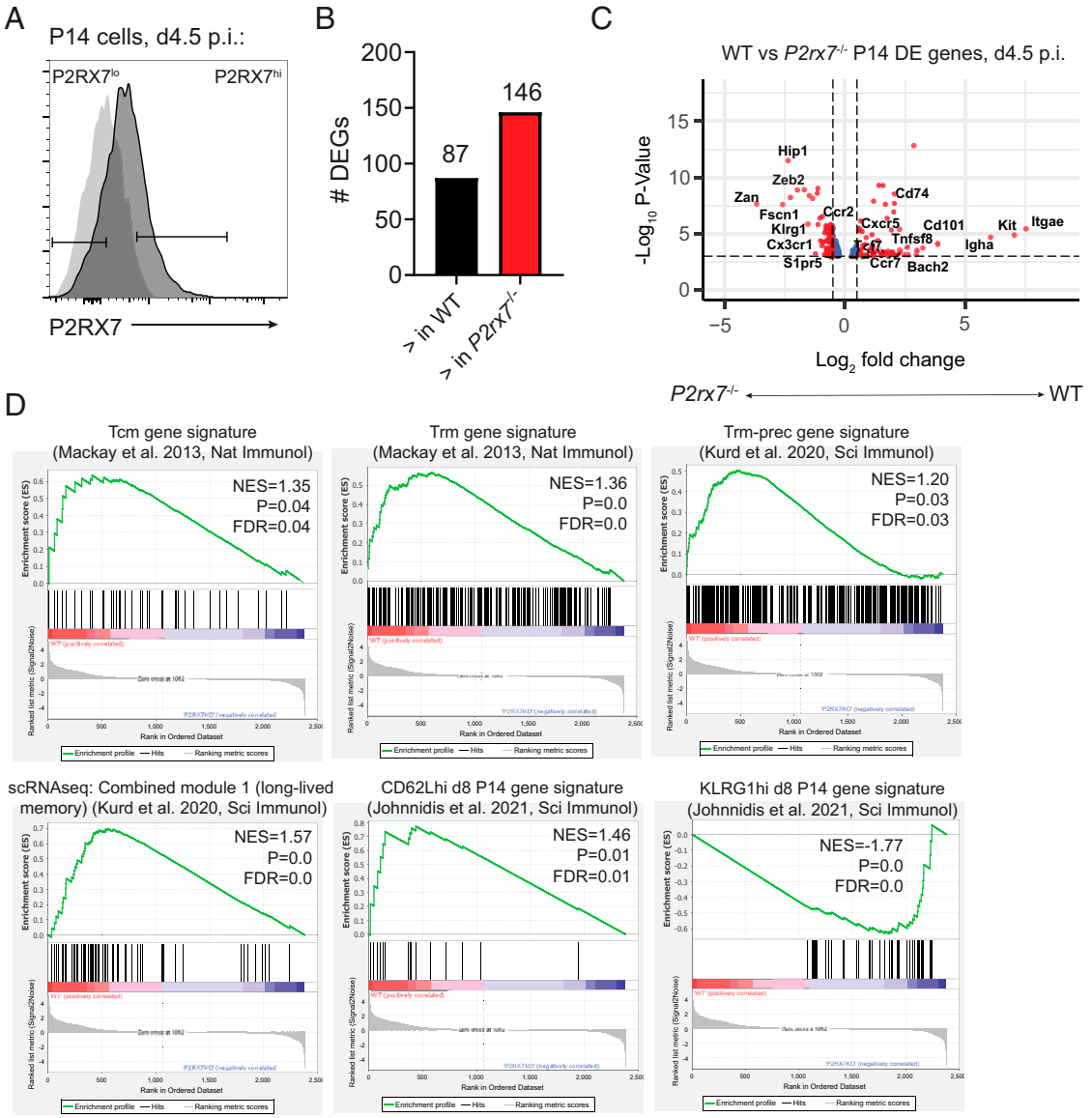

FIGURE 2. WT P14 cells are enriched for a promemory gene signature in comparison with *P2rx7*$^{-/-}$ P14 cells. (**A**) Representative flow cytometry histogram showing the expression of P2RX7 in P14 cells at day 4.5 after LCMV (dark) and naive (light gray). (**B–D**) Spleen WT and *P2rx7*$^{-/-}$ P14 cells (previously coadoptively transferred into recipient B6 mice) were sorted from recipient mice at 4.5 d after infection (p.i.). The RNAs extracted from these populations were submitted for RNA-seq analysis. (B) Bar graph showing the numbers of DEGs between WT and *P2rx7*$^{-/-}$ P14 cells. (C) Volcano plot showing all DEGs upregulated (right) or downregulated (left) in WT P14 cells compared with *P2rx7*$^{-/-}$ counterparts. Selected representative DEGs are denoted in this figure. (D) GSEA showing selected gene expression datasets (from the previous studies respectively cited) enriched in WT or *P2rx7*$^{-/-}$ (P2RX7KO) day 4.5 P14 cells. (B–D) Each replicate is a pool of spleen P14 cells from four mice; $n = 3$ replicates per experimental group. FDR, false discovery rate; NES, normalized enrichment score.

and promigration (i.e., antiresidency) pathways are enriched in *P2rx7*$^{-/-}$ early effectors (Supplemental Table I). Accompanying these characteristics, GSEA of published Tcm or Trm gene signatures revealed that many gene sets enriched in memory CD8$^+$ T cells are enriched in WT early effectors (Fig. 2D, Supplemental Table I). Conversely, gene sets represented in TE CD8$^+$ T cells were enriched in *P2rx7*$^{-/-}$ early effectors (Fig. 2D, Supplemental Table I). Therefore, the presence of P2RX7 in early effectors is associated with simultaneous memory, stemness, and residency transcriptional signatures.

We next sought to define whether not only qualitative but also quantitative differences in P2RX7 expression would differentially correlate with a promemory phenotype. We performed RNA-seq analysis of P2RX7^{hi} versus P2RX7^{lo} early effector P14 cells, which cluster differentially (Fig. 3A) and yielded >400 DEGs (Fig. 3B, 3C, Supplemental Table I). Like the WT-*P2rx7*$^{-/-}$ comparison, P2RX7^{hi} early effectors are enriched for memory CD8$^+$ T cell genes, such as *Cxcr5*, *Id3*, *Xcl1*, *Ccr7*, and *Tcf7* (Fig. 3B, 3C, Supplemental Table I), as well as Trm-specific genes such as *Nr4a2* (Fig. 3B, 3C, Supplemental Table I), whereas P2RX7^{lo} early effectors are enriched either with TE genes (e.g., *Zeb2*, *Klrg1*, *Cx3cr1*) or antiresidency genes such as *Klf2* or *S1pr1* (Fig. 3B, Supplemental Table I). Again, this was reflected in the pathways enriched in P2RX7^{hi} or P2RX7^{lo} early effectors. Although P2RX7^{hi} early effectors were enriched for many pathways associated with either survival or residency, P2RX7^{lo} early effectors were mainly enriched for apoptosis or TE differentiation pathways (Supplemental Table I). This was also observed by GSEA, where pro-Tcm/Trm datasets were enriched in P2RX7^{hi} early effectors and pro-TE phenotype datasets were enriched in P2RX7^{lo} cells (Fig. 3D, Supplemental

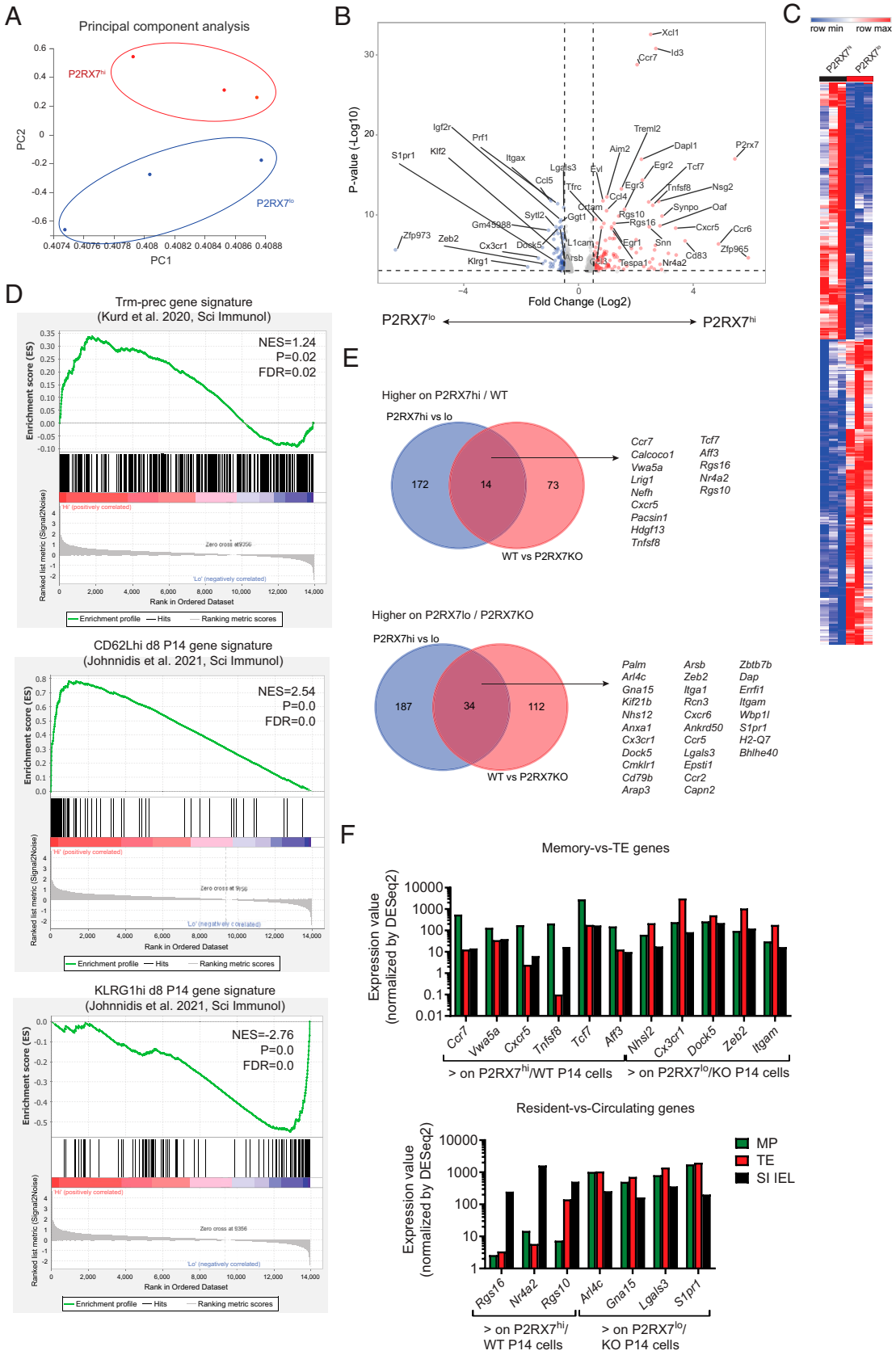

FIGURE 3. Defining the core genes quantitatively and qualitatively controlled by P2RX7 in early effector CD8$^+$ T cells. (**A**–**D**) Spleen WT P14 cells (previously transferred into recipient B6 mice) were sorted from recipient mice at 4.5 d after infection based on 20% highest (P2RX7^{hi}) and 20% lowest (P2RX7^{lo}) expression. The RNAs extracted from these populations were submitted for RNA-seq analysis. (A) Principal component (PC) analysis plot showing the relationship (based on PC1 and PC2 values) between P2RX7^{hi} and P2RX7^{lo} RNA-seq samples. (B) Volcano plot showing all DEGs upregulated (right) or downregulated (left) in P2RX7^{hi} P14 cells compared with P2RX7^{lo} counterparts. Selected representative DEGs are denoted in this figure. (C) Heatmap showing the RNA count levels (normalized Z-scores) of all DEGs between P2RX7^{hi} and P2RX7^{lo} WT P14 cells. *(Figure legend continues)*

Table I). Thus, not only P2RX7 presence but also its expression level is related to a simultaneous acquisition of memory and residency transcriptional signatures in early effector CD8$^+$ T cells. From these two analyses, we defined lists of genes that, at the early effector phase, are (1) exclusively affected by P2RX7 presence, (2) exclusively affected by P2RX7 expression level, and (3) affected by both P2RX7 presence and expression level (Fig. 3E, Supplemental Table I). Once again, among genes affected by both quantitative and qualitative P2RX7 differences, we found both memory versus TE-associated genes (e.g., *Ccr7*, *Tcf7*, *Zeb2*, *Cx3cr1*) and tissue-resident versus circulating CD8$^+$ T cell–associated genes (e.g., *Nr4a2*, *Rgs10*, *Rgs16*, *S1pr1*) (Fig. 3E, 3F).

Next, we assessed the protein levels of many of the DEGs found in the RNA-seq analyses. In early effector spleen P14 cells, a small proportion of cells express high levels of CD62L (Fig. 4A). A *t*-distributed stochastic neighbor embedding analysis revealed that, among early effectors, the highest expression of P2RX7 correlates with CD62L and inversely correlates with KLRG1 (Fig. 4A). Indeed, P2RX7^{hi} early effector P14 cells display increased levels of the memory-associated molecules CD62L, CXCR5, CD101, and CD103 compared with P2RX7^{lo} early effectors (Fig. 4B). In addition, CD44, CD8α, and the inhibitory molecule PD1 are also increased in P2RX7^{hi} early effectors (Fig. 4B). In counterpart, P2RX7^{lo} early effector P14 cells displayed enhanced expression of CD25, KLRG1, and Tim3 (Fig. 4B). P2RX7^{hi} early effector P14 cells also have increased mitochondrial membrane potential (TMRE) and mitochondrial mass (MTG) (Fig. 4C), suggesting that upregulation of P2RX7 promotes increased mitochondrial fitness at this stage. The increased levels of CD25 in day 4.5 P2RX7^{lo} P14 cells are also observed at an earlier time point, day 3 after LCMV; in contrast, these differences are not observed anymore when TEs and MPs are assessed (Fig. 4D). Agreeing with the more exacerbated differences in CD25 expression at early effector CD8$^+$ T cells, microarray data from a previous report (38) where day 3 CD25^{hi} versus day 3 CD25^{lo} cells are compared shows that P2RX7 is almost exclusively upregulated in CD25^{lo} early effectors (Fig. 4E). In addition, GSEA using defined DEGs from day 3 CD25^{hi} versus CD25^{lo} early effectors shows enrichment of CD25^{hi} early effector genes in P2RX7-deficient early effectors and a converse enrichment of CD25^{lo} genes in P2RX7-expressing early effectors (Fig. 4F).

Overall, we observed that P2RX7 heterogeneous expression in early effector CD8$^+$ T cells associates with the simultaneous acquisition of a Tcm/Trm protein and transcriptional signature.

High P2RX7 expression favors the establishment of long-lived memory CD8$^+$ T cells

Our transcriptional and protein data suggest that preferential P2RX7 expression among early effectors would favor the establishment of both Tcm and Trm CD8$^+$ T cells. To investigate this hypothesis, we sorted P2RX7^{hi} and P2RX7^{lo} early effector spleen P14 cells and adoptively transferred these cells into infection-matched secondary hosts (Fig. 5A). In synchrony with our previous data, P2RX7^{hi} progeny more efficiently established memory populations in the spleen (Fig. 5B), with a trend for preferential enrichment of Tcm cells, although percentage-wise this did not reach significance (Fig. 5B). Tem establishment (but not LLECs) was also enriched in P2RX7^{hi} progenies (Fig. 5B). The Tcm progeny from P2RX7^{hi} early effectors partially downregulated P2RX7 (Fig. 5C), although its average population expression was still substantially higher than the P2RX7^{lo} progeny, which never upregulated P2RX7 (Fig. 5C, 5D). The Tem progeny from P2RX7^{hi} early effectors also displayed increased P2RX7 compared with P2RX7^{lo} daughter cells (Supplemental Fig. 2C), which is not true in LLEC daughter cells (Supplemental Fig. 2D). At a late memory time point, we observed a further separation between the numbers of P2RX7^{hi} and P2RX7^{lo} progeny populations, and, at this point, a preferential enrichment of P2RX7^{hi}-derived Tcm cells was observed (Fig. 5E). At this time point, numerical differences between P2RX7^{hi} and P2RX7^{lo} progenies were significant for Tem cells and even for LLECs, although the magnitude of the difference is smaller than the Tcm pool (Fig. 5E), which explains the preferential enrichment of P2RX7^{hi}-derived Tcm cells. The P2RX7 bifurcation in early effectors also affected their ability to establish Trm populations, as observed in the SI IELs (Fig. 5F), liver (Supplemental Fig. 2A), and SGs (data not shown). Similarly to Tcm populations, we also observed an increased decay of P2RX7^{lo} progenies in the SI IEL Trm pool at late memory (Fig. 5F), although no differences in P2RX7 expression were observed between SI IEL transferred cells (Supplemental Fig. 2B). The differential decay of P2RX7^{hi} versus P2RX7^{lo} early effector progenies is better exemplified in Fig. 5G.

Not only the accumulation but also the quality of Tcm and Trm cells is distinct in P2RX7^{hi} versus P2RX7^{lo} progenies. In response to ex vivo restimulation, P2RX7^{hi} daughter cells produce significantly lower levels of IFN-γ and a trend for lower GzmB (Fig. 5H), which are hallmarks of quiescent Tcm cells. Moreover, mitochondrial membrane potential and mitochondrial mass are both increased in P2RX7^{hi}-derived Tcm cells (Fig. 5I); the increased levels of mitochondrial membrane potential are also observed in P2RX7^{hi}-derived SI IEL Trm cells (Fig. 5I). We sought to test the ability of Trm daughter cells to produce cytokines and to respond to TGF-β ex vivo. These attempts were unsuccessful due to extensive SI IEL T cell death in ex vivo cultures, paired with the already low numbers of donor cells (data not shown). Instead, we tested how P2RX7^{hi} versus P2RX7^{lo} early effectors respond to TGF-β ex vivo as a readout of the ability of these cells to respond to the Trm-driving factor TGF-β. These experiments evidenced that P2RX7^{hi} early effectors are significantly better in their ability to upregulate CD103 protein expression, a typical marker of Trm cells and a common readout of TGF-β–induced responses (Fig. 5J). Altogether, these results indicate that high P2RX7 expression in early effector CD8$^+$ T cells preferentially favors the generation of long-lived Tcm and Trm cells.

Zeb2 *knockdown preferentially rescues the memory CD8$^+$ T cell pool in P2RX7-deficient CD8$^+$ T cells*

Among the genes affected by quantitative and qualitative P2RX7 expression differences in early effector CD8$^+$ T cells, we found *Zeb2*, which encodes the zinc finger transcriptional repressor Zeb2. This protein, which is expressed at higher levels in TEs relative to MPs (Supplemental Table I, Fig. 3F), promotes the TE phenotype at the expense of the memory CD8$^+$ T cell pool (39–41). Given that *Zeb2* was higher in P2RX7-deficient or P2RX7^{lo} early effector CD8$^+$ T cells, we speculated that *Zeb2* ablation would preferentially

(D) GSEA showing selected gene expression datasets (from the previous studies respectively cited) enriched in P2RX7^{hi} or P2RX7^{lo} day 4.5 P14 cells. (**E**) Venn diagrams showing the correlation between DEGs found between WT and *P2rx7*$^{-/-}$ day 4.5 P14 cells (red) and P2RX7^{hi} versus P2RX7^{lo} day 4.5 P14 cells (blue). The common DEGs found for both these comparisons (purple intersections) are listed. (**F**) Immgen (https://www.immgen.org/) RNA expression values (day 7 MPs, TEs, or SI-IEL P14) of selected genes enriched (in our analysis) in WT/P2RX7^{hi} day 4.5 P14 cells or *P2rx7*$^{-/-}$/P2RX7^{lo} day 4.5 P14 cells. (A–D) Each replicate is a pool of spleen P14 cells from six mice; $n = 3$ replicates per experimental group. FDR, false discovery rate; NES, normalized enrichment score.

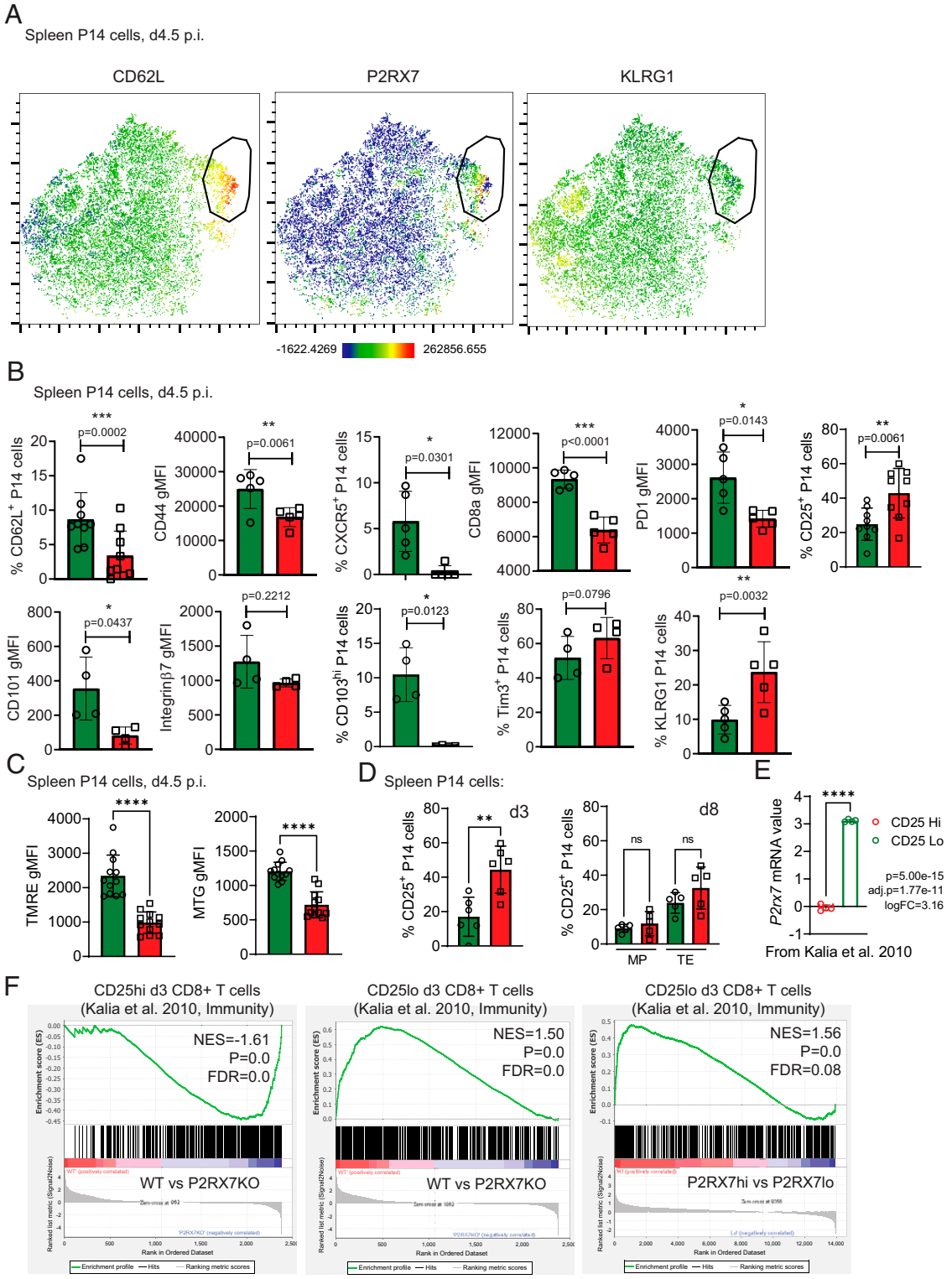

FIGURE 4. P2RX7 protein expression in early effector CD8$^+$ T cells correlates with memory marker expression. (**A**–**D**) WT P14 cells were adoptively transferred into recipient B6 mice, which were infected with LCMV-Arm. Infected mice spleens were harvested at day 4.5 (A–C), day 3, or day 8 (D) after infection (p.i.) for P14 cell analysis. (A) Representative *t*-distributed stochastic neighbor embedding plots depicting the protein expression of CD62L, P2RX7, and KLRG1 among spleen P14 cells. (B) Average values for percentages of CD62L$^+$/CXCR5$^+$/CD25$^+$/CD103^{hi}/Tim3$^+$/KLRG1$^+$ and CD44/CD8α/PD1/CD101/integrin β7 geometric mean fluorescence intensity (gMFI) in P2RX7^{hi} and P2RX7^{lo} spleen P14 cells. (C) Average gMFI values for TMRE and MTG in P2RX7^{hi} and P2RX7^{lo} spleen P14 cells. (D) Average percentages of CD25$^+$ P2RX7^{hi} and P2RX7^{lo} spleen P14 cells at day 3 after LCMV (left) and of CD25$^+$ P2RX7^{hi} and P2RX7^{lo} spleen P14 MPs and TEs at day 8 after LCMV (right). (**E**) *P2rx7* mRNA values from day 3 post-LCMV CD25^{hi} versus CD25^{lo} P14 cells [data taken from Ref. (38)]. (**F**) GSEA showing the listed gene expression datasets [data taken from Ref. (38)] enriched in day 4.5 WT or P2RX7-KO P14 cells (left and center) and in day 4.5 P2RX7^{hi} versus P2RX7^{lo} P14 cells (right). (B–E) Unpaired *t* test; $*p < 0.05$, $**p < 0.01$, $***p < 0.001$, and $****p < 0.0001$. (D, right) One-way ANOVA. (B–D) Average values ± SD; data pooled from two or three independent experiments ($n = 5$–10).

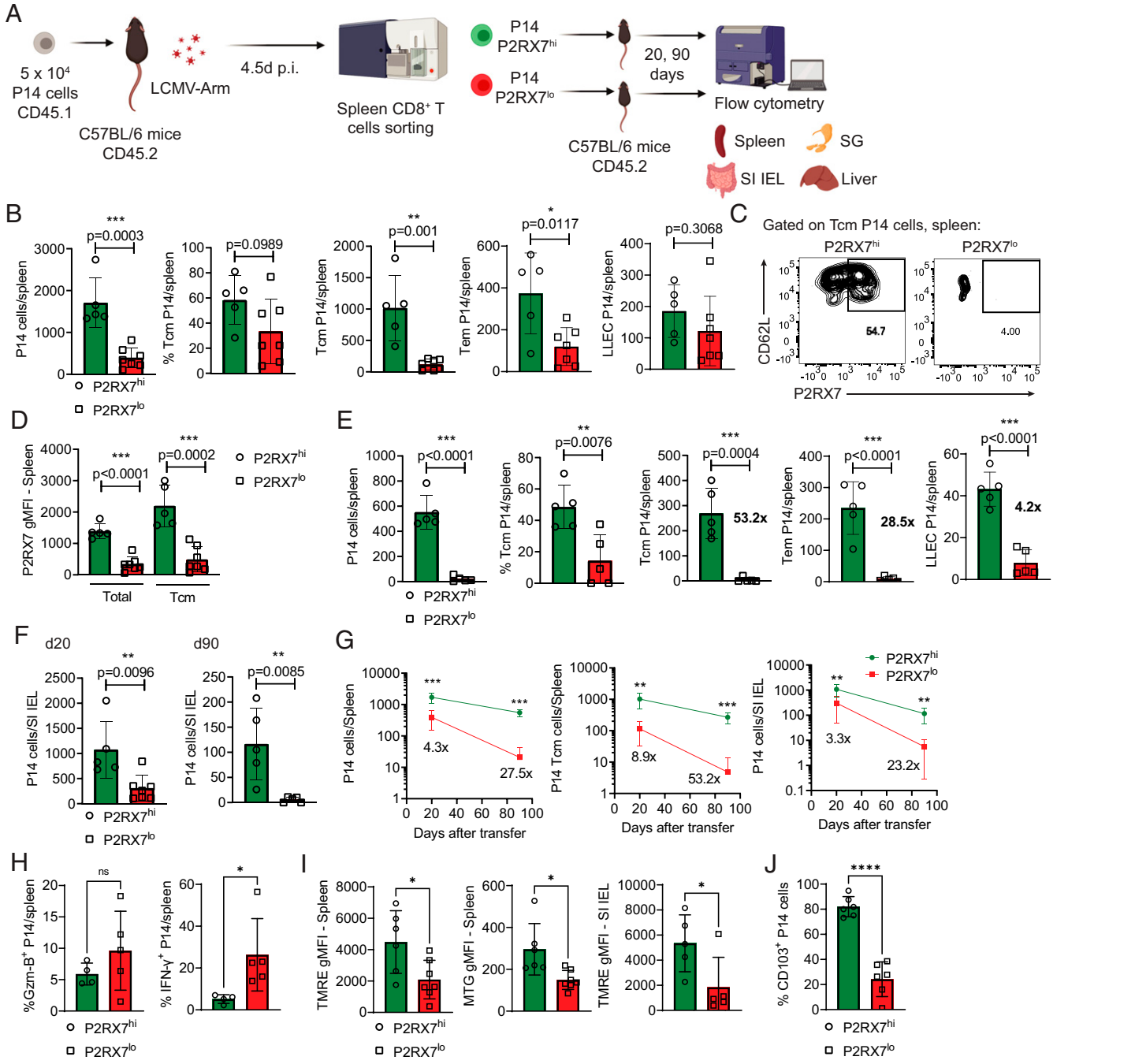

FIGURE 5. P2RX7 expression in early effectors favors the establishment of long-lived circulating and resident memory CD8$^+$ T cells. (**A–J**) P14 cells were adoptively transferred into B6 mice (infected with LCMV-Arm), and, at day 4.5 after infection (p.i.), P2RX7^{hi} (20% highest) and P2RX7^{lo} (20% lowest) were sorted and adoptively transferred into infection-matched mice (3×10^5 cells/mouse). At days 20 and 90 after transfer, secondary recipient mice were assessed for transferred P14 cell numbers and phenotype. (A) Experimental plan for the secondary transfer experiments. (B) Total numbers, percentages of Tcm, and numbers of Tcm/Tem/LLEC P14 cells from P2RX7^{hi} or P2RX7^{lo} early effector progenitors at day 20 after transfer. (C) Representative flow cytometry plots showing P2RX7 expression in Tcm P14 cells from P2RX7^{hi} and P2RX7^{lo} early effectors at day 20 after transfer. (D) Average P2RX7 geometric mean fluorescence intensity (gMFI) levels in total and Tcm spleen P14 cells from P2RX7^{hi} and P2RX7^{lo} donors at day 20 after transfer. (E) Total numbers, percentages of Tcm, and numbers of Tcm/Tem/LLEC P14 cells from P2RX7^{hi} or P2RX7^{lo} early effector progenitors at day 90 after transfer. (F) Numbers of SI IEL P14 cells at day 20 (left) and day 90 (right) after transfer. (G) Kinetics of the numbers of total spleen (left), spleen Tcm (center), and SI IEL (right) P14 cells over time after secondary transfer. The fold differences between P2RX7^{hi} and P2RX7^{lo} donor P14 cells are shown. (H) Percentages of GzmB$^+$ and IFN-γ$^+$ P14 cells from P2RX7^{hi} or P2RX7^{lo} early effectors at day 20 after transfer. (I) Average gMFI values for TMRE (left) and MTG (center) in spleen P14 cells and TMRE from SI IEL P14 cells (right) from P2RX7^{hi} or P2RX7^{lo} early effectors at day 20 after transfer. (J) Average percentages of CD103$^+$ P14 cells from P2RX7^{hi} or P2RX7^{lo} early effector donors after 40-h incubation with TGF-β. (B, D–J) Unpaired *t* test; $^*p < 0.05$, $^{**}p < 0.01$, $^{***}p < 0.001$, $^{****}p < 0.0001$. (B–J) Average values ± SD; data pooled from three independent experiments ($n = 5–7$).

rescue memory CD8$^+$ T cell generation in the absence of P2RX7. To test this, we used RNP-based CRISPR-Cas9 to knock out *Zeb2* in WT or P2RX7-deficient P14 cells (Fig. 6A). The efficiency of *Zeb2* KO was 82.9%, on average, as shown in Supplemental Fig. 3A. *Zeb2* KO, as previously described (39–41), significantly repressed the ability of WT P14 cells to differentiate into KLRG1$^+$

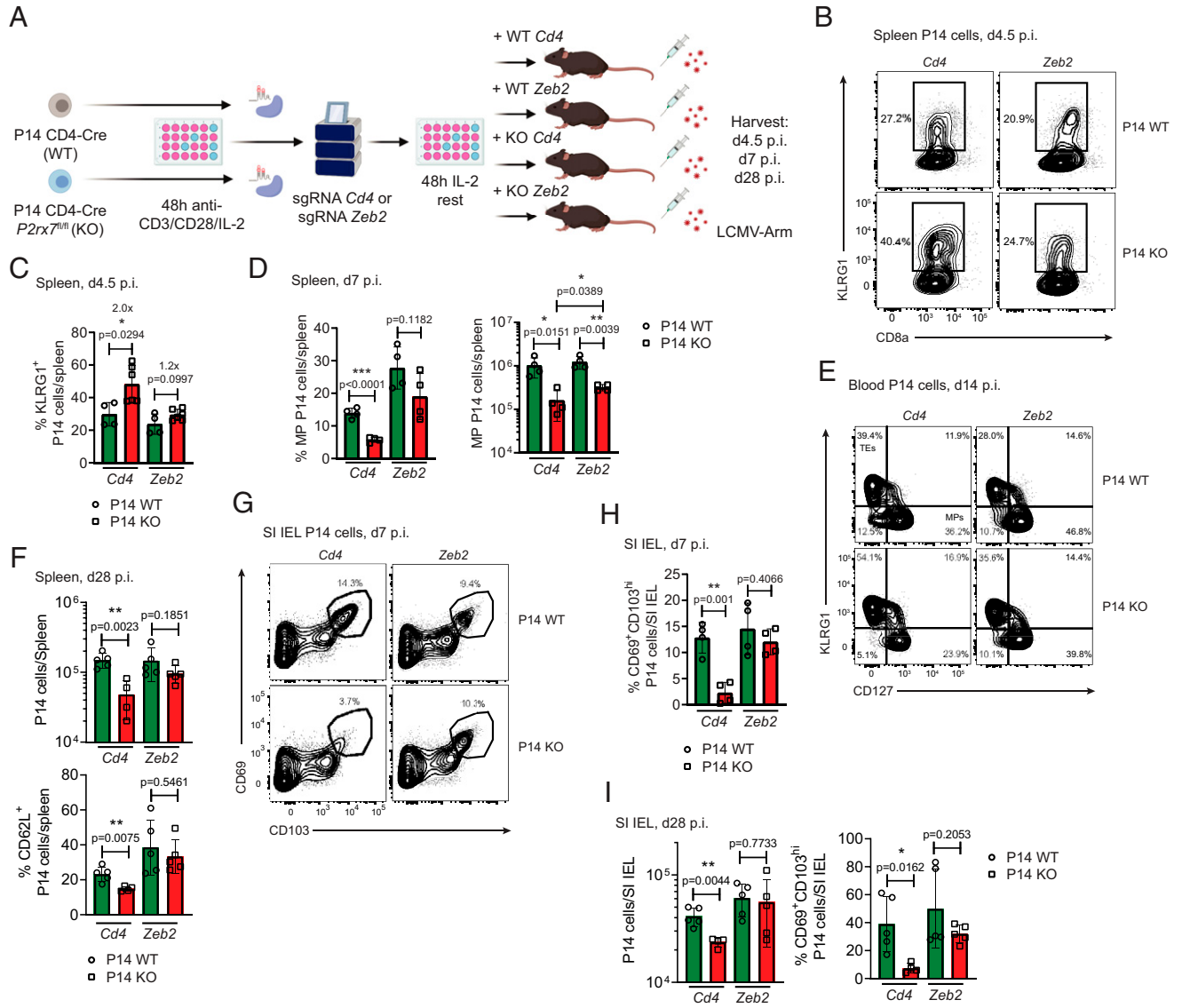

FIGURE 6. *Zeb2* KO partially rescues the ability of P2RX7-deficient CD8$^+$ T cells to form early MPs and Tcm and Trm subsets. (**A–I**) WT (CD4-Cre) and P2RX7-KO (CD4-Cre *P2rx7*$^{fl/fl}$) P14 cells were in vitro activated. After 48 h, CRISPR-Cas9 RNP-based knockdown of *Zeb2* or *Cd4* (control) was performed. Cells were rested in IL-2 for an additional 48 h and subsequently transferred into recipient B6 mice. Recipient mice were infected with LCMV-Arm, and the numbers and phenotype of transferred P14 cells were assessed over time after infection (p.i.). (A) Experimental strategy of the CRISPR-Cas9 knockdown experiments. (B) Representative flow cytometry plots showing expression of KLRG1 in spleen P14 cells at day 4.5 after infection. (C) Percentages of spleen KLRG1$^+$ P14 cells at day 4.5 after infection. (D) Percentages (top) and numbers (bottom) of KLRG1$^-$CD127$^+$ MP P14 cells in the spleen at day 7 after infection. (E) Representative flow cytometry plots showing expression of KLRG1 and CD127 in blood P14 cells at day 14 after infection. (F) Total numbers (top) and percentages of Tcm (CD62L$^+$; bottom) spleen P14 cells at day 28 after infection. (G) Representative flow cytometry plots showing the expression of CD69 and CD103 in SI IEL P14 cells at day 7 after infection. (H) Percentages of CD69$^+$CD103^{hi} SI IEL P14 cells at day 7 after infection. (I) Total numbers (top) and percentages of CD69$^+$CD103^{hi} (bottom) SI IEL P14 cells at day 28 after infection. (C, D, F, H, I) Unpaired *t* test; $*p < 0.05$, $**p < 0.01$, and $***p < 0.001$. (B–I) Average values ± SD; data pooled from two independent experiments ($n = 4–6$).

early effectors or TEs at peak effector phase (Fig. 6B, 6C, 6E, Supplemental Fig. 3B). *Zeb2* KO in WT P14 cells promoted the MP phenotype and, after the early effector phase, the percentage of CD62L$^+$ P14 cells (Fig. 6D, 6E, Supplemental Fig. 3C), but it did not lead to any numerical expansion of these populations (Fig. 6D, Supplemental Fig. 3D). In contrast, *Zeb2*-ablated P2RX7-KO P14 cells not only showed a diversion toward the MP phenotype in terms of percentage but also displayed a significant numerical increase in MPs (Fig. 6B–6E, Supplemental Fig. 3B–3D). This scenario was also observed at the memory time point. In WT P14 cells, *Zeb2* KO induced a mild increase in the percentage of Tcm populations (and a decrease in LLECs) (Fig. 6F, Supplemental Fig. 3E), but this was not accompanied by changes in the number of memory P14 cells observed (Fig. 6F, Supplemental Fig. 3D). *Zeb2*-ablated P2RX7-KO P14 cells, in contrast, not only underwent more profound alterations in the proportions of Tcm and LLECs observed (Fig. 6F, Supplemental Fig. 3E) but also accumulated in higher numbers, such that there was no longer a statistical difference between WT and P2RX7-KO populations in the frequency of Tcm (Fig. 6F, Supplemental Fig. 3D). *Zeb2* KO therefore led to a disproportionate rescue of the ability of P2RX7-deficient CD8$^+$ T cells to differentiate into circulating memory cells, especially the Tcm pool.

When Trm generation in the presence of *Zeb2* ablation was assessed, even more pronounced differences were observed. The

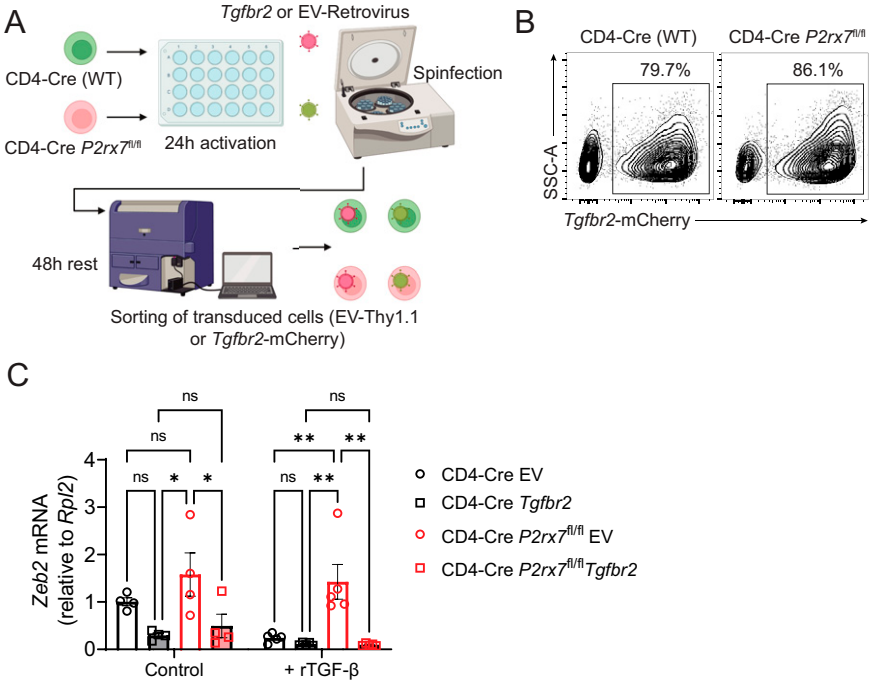

FIGURE 7. *Tgfbr2* overexpression compensates the deficiency in P2RX7 for the suppression of *Zeb2* expression in effector CD8$^+$ T cells. (**A**–**C**) WT (CD4-Cre) and P2RX7-KO (CD4-Cre *P2rx7*$^{fl/fl}$) P14 cells were in vitro activated. After 24 h, cells were transduced with control empty retrovirus (RV-EV; expressing Thy1.1) or *Tgfbr2*-encoding retrovirus (RV-*Tgfbr2*; expressing mCherry) via spinfection. Cells were rested for 48 h and then sorted on the basis of transduction markers Thy1.1 or mCherry. Sorted, transduced cells were incubated for 40 h with TGF-β. (A) Schematics of the experimental design. (B) Representative flow cytometry plots showing mCherry expression (as a readout for transduction with RV-*Tgfbr2*) in WT or P2RX7-KO P14 cells before cell sorting (above) and after cell sorting (below). (C) Average *Zeb2* mRNA expression values in RV-EV– and RV-*Tgfbr2*–transduced WT and P2RX7-KO P14 cells after incubation with TGF-β. (C) One-way ANOVA; $*p < 0.05$, $**p < 0.01$. (C) Average values ± SD; data pooled from three independent experiments ($n = 6$). SSC-A, side scatter area.

initial tissue infiltration in SI IELs by total P14 cells was not affected by either P2RX7 KO (25) or *Zeb2* ablation (Supplemental Fig. 3F). However, the differentiation of CD69^{hi}CD103^{hi} cells, which we previously identified to be largely absent in P2RX7-KO cells (25), was almost completely rescued when *Zeb2* was ablated (Fig. 6G, 6H). This was also observed at memory time points, where a numerical rescue of P2RX7-KO SI IEL Trm generation was also observed when *Zeb2* knockdown occurred (Fig. 6I). The infiltration and accumulation of P2RX7-KO SG P14 cells were also rescued by *Zeb2* knockdown (Supplemental Fig. 3G, 3H). Overall, our data strongly indicate that P2RX7 promotes systemic virus-specific Tcm and Trm cells through inducing a promemory signature that is at least partly dependent on *Zeb2* negative regulation. It is of note that Zeb2, although a transcriptional repressor, did not directly affect P2RX7 expression in either circulating or Trm populations (Supplemental Fig. 3I–3K).

P2RX7 upregulation leads to repression of Zeb2 via TGF-β signaling in early effector CD8$^+$ T cells

Our data suggest that P2RX7 induces a pro-Tcm/Trm fate through negative regulation of the expression of Zeb2, a promoter of the TE fate (39, 41). We have previously shown that P2RX7-induced responses to TGF-β are important for the establishment of memory CD8$^+$ T cells, such that overexpression of its receptor TGF-βRII (encoded by *Tgfbr2*) using retroviral delivery rescued the ability of P2RX7-KO P14 cells to develop Tcm and Trm populations (25). Importantly, Zeb2 has been shown to be inhibited by TGF-β signaling in CD8$^+$ T cells, which favors the acquisition of a memory phenotype (40). On this basis, we hypothesized that P2RX7 favors the Tcm/Trm fate in early effectors through inhibition of Zeb2 expression via increasing CD8$^+$ T cell sensitivity to TGF-β. To test this, we overexpressed *Tgfbr2* in WT and P2RX7-KO P14 cells and sorted transduced cells for in vitro cultures in the presence of TGF-β (Fig. 7A, 7B). *Zeb2* mRNA expression, which is already diminished in WT cells in comparison with KO cells in the absence of TGF-β, is further suppressed in TGF-β–treated WT cells, which is not observed in P2RX7-KO P14 cells (Fig. 7C, left). Overexpression of *Tgfbr2*, in contrast, rendered P2RX7-KO P14 cells to repress *Zeb2* expression, leading to a preferential "rescue" in their ability to suppress expression of this transcriptional repressor; this is only true when P14 cells are exposed to TGF-β (Fig. 7C, right). Together, these results indicate that unequal P2RX7 induction at the early effector stage induces the negative regulation of Zeb2 expression (and subsequently the Tcm/Trm fate) at least in part through increasing the ability of early effector CD8$^+$ T cells to respond to TGF-β.

Discussion

Sensing of microenvironmental changes plays a key role in the activation of many immune cells. CD8$^+$ T cells are not different, because they express many receptors for extracellular signals. Those receptors include, evidently, cytokine and chemokine receptors (19, 42). In addition, receptors for extracellular molecules released during infection are also expressed by CD8$^+$ T cells during immune responses. One example is eATP, which can be released actively through exporting channels, such as pannexin-1 (43, 44), or passively by dying cells due to local or systemic inflammation and tissue damage (23). One eATP sensor in particular (P2RX7) is expressed at high levels and plays relevant roles in controlling CD8$^+$ T cell responses (24, 25, 45, 46). Because eATP can be released actively or passively, it is possible that CD8$^+$ T cells are exposed to this signal not only at sites of active viral infection but also in secondary lymphoid organs during initial effector function. In agreement with this notion, P2RX7 is quickly upregulated in early effector CD8$^+$ T cells (25). In our study, we further explored this and found that P2RX7 upregulation in some early effectors favors the acquisition of transcriptional and protein memory signatures shared by Tcm and Trm cells. These findings suggest that the simultaneous promotion of Tcm and Trm cells by P2RX7 can be explained, at least in part, by differential sensing of eATP by early effector CD8$^+$ T cells, which promote the generation of early MPs among some of these cells.

Previous reports have suggested that a minor fraction of early effector CD8$^+$ T cells display heightened ability to differentiate into long-lived memory cells (12–14, 16). These studies mostly have focused on the transcriptional regulation of this subset and have

defined an important role for many transcriptional factors, especially TCF-1 (13, 15, 16). These studies have also identified many receptors that, regardless of being controlled by TCF-1 or not, are associated with the memory fate. Whether these receptors for extracellular signals actively play a role in the early differentiation into MPs is unclear. Our results show that P2RX7 is one of these receptors and that it actively promotes the diversion into the memory phenotype. Expression of P2RX7 and TCF-1 correlates in both $CD8^+$ T cell early effectors and MPs. The hierarchy between TCF-1 and P2RX7 expression, however, is currently unclear. P2RX7 is upregulated in effector $CD8^+$ T cells before TCF-1 reexpression (25), which at first suggests that P2RX7 antecedes TCF-1. Yet, a report using chronic LCMV suggests TCF-1 can bind to the *P2rx7* enhancer locus in $CD8^+$ T cells (47). Alternatively, a positive feedback mechanism may occur. In this situation, P2RX7 signaling in some early effectors may help the reexpression of TCF-1, and simultaneously TCF-1 reinforces the preferential upregulation of P2RX7. Future research will be needed to better define whether and how TCF-1 reexpression solidifies the preferential P2RX7 expression in early MPs.

Our data show that differences in P2RX7 expression between $CD8^+$ T cells occurs at the early effector phase, and it favors the later accumulation of memory $CD8^+$ T cells to a point that, even more than their initial accumulation, P2RX7 early bifurcation influences the ability of memory $CD8^+$ T cells to maintain in the long term. Our current data tracked these differences at the earliest time when peak P2RX7 expression in effector $CD8^+$ T cells happens: at days 4 and 5 after LCMV infection (25). However, P2RX7 upregulation can be detected as early as 2 d after LCMV or in vitro activation (25). It is possible, therefore, that asymmetrical distribution of P2RX7 at even earlier time points may help direct the memory versus TE programs in $CD8^+$ T cells. Many studies have reported that asymmetrical partitioning of proteins in $CD8^+$ T cells early after Ag priming favors the generation of memory cells in some daughters in detriment of the others (48–51). More specifically, asymmetric inheritance of TCF-1, T-bet, and mammalian target of rapamycin complex 1 were all associated with these outcomes (17, 18, 49, 52). Aside from the possible connection between TCF-1 and P2RX7, in our previous study, we have shown P2RX7 expression in memory $CD8^+$ T cells is inversely correlated with mammalian target of rapamycin pathway activation (24). Whether this is also true at the beginning of immune responses remains to be defined and may offer a further mechanistic basis for the differentiation of $P2RX7^{hi}$ $CD8^+$ T cells in early MPs.

In contrast with the potential for early asymmetrical division to differentially promote memory versus TEs, other reports suggest that memory $CD8^+$ T cells arise from dedifferentiated effector $CD8^+$ T cells (53, 54). This apparent discrepancy may, on one side, reflect distinct experimental approaches or Ag stimulation nature. Alternatively, they may reflect heterogeneity in the memory $CD8^+$ T cell populations formed in response to a determined Ag. Our results, indeed, showed that even $P2RX7^{lo}$ early effectors or MPs can form memory populations, although less efficiently. Given that $P2RX7^{lo}$ early effectors display a pro-TE phenotype, these results suggest that even some TE-leaning $CD8^+$ T cells can revert their phenotype toward memory, which has been reported previously (55). Therefore, our division between $P2RX7^{hi}$ and $P2RX7^{lo}$ early effectors may define cells that develop into memory through early differentiation events and cells that develop into memory via dedifferentiation during T cell contraction.

Another unclear point is the dynamic changes we observed in P2RX7 expression after the early effector phase. The progeny from $P2RX7^{lo}$ early effectors found in the circulation never upregulated P2RX7, even the few that developed into Tcm cells. In contrast, $P2RX7^{lo}$ MPs were able to upregulate P2RX7. This suggests a complex expression control network, where low expression of P2RX7 at the early effector phase is accompanied by modifications that prevent its upregulation later. A possibility is that differential expression of P2RX7 is related to or promotes epigenetic modifications in its own locus. Epigenetic modifications have been described to imprint numerous phenotypes in effector versus memory $CD8^+$ T cells, with potential roles attributed to Tet and histone deacetylase epigenetic modulators (56–58). Of note, histone deacetylase–related gene sets were enriched in $P2RX7^{lo}$ early effector $CD8^+$ T cells. Whether epigenetic alterations at the *P2rx7* locus explain this expression dynamic remains to be defined. Nevertheless, this should not be related to P2RX7 expression in Trm cells, because even the few $P2RX7^{lo}$ early effectors differentiating into Trm cells express high levels of P2RX7. In this case, other signaling pathways and transcriptional controllers may function in the *P2rx7* locus after nonlymphoid tissue entry, such as retinoic acid signaling (59).

The acquisition of a Trm cell potential, although possibly requiring additional signals after nonlymphoid tissue entry (25, 26, 60), is potentially imprinted in certain circulating early effector $CD8^+$ T cells (61). The nature of this imprint is not clear, however. It may, on one side, rely on stochastic signals sensed by a subset of early effectors, regardless of TCR differences (11). Alternatively, it may reflect distinct TCR functional avidities and/or affinities, as recently suggested (61). The extracellular signals promoting this imprinting are also not fully explored. Our previous report suggested that P2RX7-mediated eATP sensing may favor the subsequent generation of Trm precursors (25). Here, we not only confirmed these findings but also provided additional evidence that P2RX7 asymmetrical expression in early effectors already aligned with transcriptional differentiation involving certain residency-versus-circulation signatures. They do not exclude, by any means, the likelihood that eATP sensing through P2RX7 also plays a role in Trm generation after nonlymphoid tissue entry, which our previous report also suggested as a mechanism for the function of this receptor (25). Rather, the presence of Trm cells from P2RX7-imprinted versus nonimprinted early effectors may reflect heterogeneous populations forming in nonlymphoid tissues. Our results showed that $P2RX7^{hi}$-derived Trm cells tended to survive longer, which suggests that P2RX7 signaling at the early effector phase promotes a longer-lived subset of Trm cells. In agreement with this notion, two recent reports have shown *P2rx7* differentially expressed in an SI IEL–infiltrating $CD8^+$ T cell subset that also contained long-lived memory-associated genes (10, 60). Whether P2RX7 signaling in early effectors preferentially gives rise to a long-lived subset of Trm cells remains to be defined and is a current goal of our group.

We have found that P2RX7 high expression at the early effector phase was negatively correlated with *Zeb2* expression. Zeb2 directly promotes the TE/LLEC phenotype at the expense of memory $CD8^+$ T cell subsets, but without major effects in the total numbers of memory $CD8^+$ T cells formed (39, 41). In contrast with these previous reports, *Zeb2* ablation not only redirected the P2RX7-deficient $CD8^+$ T cell pool toward memory differentiation and away from TEs but also significantly increased the size of the memory cell population. Zeb2 ablation does not completely restore early MP generation, which indicates that other P2RX7-controlled pathways may play a role, such as the AMP kinase pathway, which we have previously studied in the context of P2RX7 deficiency (24). In the present study, the KO efficiency of Zeb2 was not complete, which makes it possible that the incomplete rescue observed in Zeb2 ablation is due to incomplete Zeb2 KO efficiency. Despite these nuances, our results suggested that Zeb2 expression is negatively controlled by P2RX7 upregulation, which we confirmed in this paper (Fig. 7). Our data also indicate that Zeb2 expression is controlled by P2RX7 upregulation indirectly, at least partly through

induction of TGF-β, which has been described to directly downregulate Zeb2 (40). We have previously found the TGF-β pathway to be enriched in P2RX7-expressing effector CD8$^+$ T cells (25). Overexpression of *Tgfbr2* almost completely rescued the ability of P2RX7-deficient effector CD8$^+$ T cells to negatively regulate Zeb2 expression, but that does not rule out other possible intermediate pathways by which P2RX7 controlled. A possible candidate for this is TCF-1, whose expression is positively correlated with P2RX7 and negatively correlated with Zeb2 and is not directly controlled by Zeb2 (39). Another signal that reportedly represses Zeb2 expression is the miR-200 microRNAs (40). In the future, more detailed studies are needed to test the possible connection between P2RX7, TCF-1, and/or miR-200 and Zeb2. The connection between P2RX7, TGF-β signaling, and Zeb2 nevertheless may help explain why *Zeb2* ablation also led to significant numerical rescue of P2RX7-deficient Trm cell generation, although the enrichment in early MPs may also explain this result.

In summary, this work highlights how differential acquisition of eATP sensing ability serves to transcriptionally promote many aspects of a promemory signature in a subset of early effector CD8$^+$ T cells. Identifying the factors precisely controlled by P2RX7-eATP sensing in early effectors will allow significant improvement of immunization against infection or cancer, including the use of T cell–targeted P2RX7 agonism as a form of promoting memory CD8$^+$ T cells in the circulation and in barrier tissues simultaneously.

Acknowledgments

We thank the members of the Borges da Silva and Jamequist laboratories for intellectual input.

Disclosures

The authors have no financial conflicts of interest.

References

1. Farber, D. L., M. G. Netea, A. Radbruch, K. Rajewsky, and R. M. Zinkernagel. 2016. Immunological memory: lessons from the past and a look to the future. *Nat. Rev. Immunol.* 16: 124–128.
2. Williams, M. A., and M. J. Bevan. 2007. Effector and memory CTL differentiation. *Annu. Rev. Immunol.* 25: 171–192.
3. Jameson, S. C., and D. Masopust. 2018. Understanding subset diversity in T cell memory. *Immunity* 48: 214–226.
4. Gerlach, C., E. A. Moseman, S. M. Loughhead, D. Alvarez, A. J. Zwijnenburg, L. Waanders, R. Garg, J. C. de la Torre, and U. H. von Andrian. 2016. The chemokine receptor CX3CR1 defines three antigen-experienced CD8 T cell subsets with distinct roles in immune surveillance and homeostasis. *Immunity* 45: 1270–1284.
5. Milner, J. J., H. Nguyen, K. Omilusik, M. Reina-Campos, M. Tsai, C. Toma, A. Delpoux, B. S. Boland, S. M. Hedrick, J. T. Chang, and A. W. Goldrath. 2020. Delineation of a molecularly distinct terminally differentiated memory CD8 T cell population. *Proc. Natl. Acad. Sci. USA* 117: 25667–25678.
6. Sallusto, F., D. Lenig, R. Förster, M. Lipp, and A. Lanzavecchia. 1999. Two subsets of memory T lymphocytes with distinct homing potentials and effector functions. *Nature* 401: 708–712.
7. Masopust, D., and A. G. Soerens. 2019. Tissue-resident T cells and other resident leukocytes. *Annu. Rev. Immunol.* 37: 521–546.
8. Mueller, S. N., and L. K. Mackay. 2016. Tissue-resident memory T cells: local specialists in immune defence. *Nat. Rev. Immunol.* 16: 79–89.
9. Szabo, P. A., M. Miron, and D. L. Farber. 2019. Location, location, location: tissue resident memory T cells in mice and humans. *Sci. Immunol.* 4: eaas9673.
10. Milner, J. J., C. Toma, Z. He, N. S. Kurd, Q. P. Nguyen, B. McDonald, L. Quezada, C. E. Widjaja, D. A. Witherden, J. T. Crowl, et al. 2020. Heterogenous populations of tissue-resident CD8$^+$ T cells are generated in response to infection and malignancy. *Immunity* 52: 808–824.e7.
11. Gaide, O., R. O. Emerson, X. Jiang, N. Gulati, S. Nizza, C. Desmarais, H. Robins, J. G. Krueger, R. A. Clark, and T. S. Kupper. 2015. Common clonal origin of central and resident memory T cells following skin immunization. *Nat. Med.* 21: 647–653.
12. Sarkar, S., V. Kalia, W. N. Haining, B. T. Konieczny, S. Subramaniam, and R. Ahmed. 2008. Functional and genomic profiling of effector CD8 T cell subsets with distinct memory fates. *J. Exp. Med.* 205: 625–640.
13. Johnnidis, J. B., Y. Muroyama, S. F. Ngiow, Z. Chen, S. Manne, Z. Cai, S. Song, J. M. Platt, J. M. Schenkel, M. Abdel-Hakeem, et al. 2021. Inhibitory signaling sustains a distinct early memory CD8$^+$ T cell precursor that is resistant to DNA damage. *Sci. Immunol.* 6: eabe3702.
14. Lin, W. W., S. A. Nish, B. Yen, Y. H. Chen, W. C. Adams, R. Kratchmarov, N. J. Rothman, A. Bhandoola, H. H. Xue, and S. L. Reiner. 2016. CD8$^+$ T lymphocyte self-renewal during effector cell determination. *Cell Rep.* 17: 1773–1782.
15. Zhou, X., S. Yu, D. M. Zhao, J. T. Harty, V. P. Badovinac, and H. H. Xue. 2010. Differentiation and persistence of memory CD8$^+$ T cells depend on T cell factor 1. *Immunity* 33: 229–240.
16. Pais Ferreira, D., J. G. Silva, T. Wyss, S. A. Fuertes Marraco, L. Scarpellino, M. Charmoy, R. Maas, I. Siddiqui, L. Tang, J. A. Joyce, et al. 2020. Central memory CD8$^+$ T cells derive from stem-like Tcf7^{hi} effector cells in the absence of cytotoxic differentiation. *Immunity* 53: 985–1000.e11.
17. Pollizzi, K. N., I. H. Sun, C. H. Patel, Y. C. Lo, M. H. Oh, A. T. Waickman, A. J. Tam, R. L. Blosser, J. Wen, G. M. Delgoffe, and J. D. Powell. 2016. Asymmetric inheritance of mTORC1 kinase activity during division dictates CD8$^+$ T cell differentiation. *Nat. Immunol.* 17: 704–711.
18. Verbist, K. C., C. S. Guy, S. Milasta, S. Liedmann, M. M. Kamiński, R. Wang, and D. R. Green. 2016. Metabolic maintenance of cell asymmetry following division in activated T lymphocytes. *Nature* 532: 389–393.
19. Schenkel, J. M., K. A. Fraser, K. A. Casey, L. K. Beura, K. E. Pauken, V. Vezys, and D. Masopust. 2016. IL-15-independent maintenance of tissue-resident and boosted effector memory CD8 T cells. *J. Immunol.* 196: 3920–3926.
20. Mueller, S. N., and R. Ahmed. 2008. Lymphoid stroma in the initiation and control of immune responses. *Immunol. Rev.* 224: 284–294.
21. Leal, J. M., J. Y. Huang, K. Kohli, C. Stoltzfus, M. R. Lyons-Cohen, B. E. Olin, M. Gale, Jr., and M. Y. Gerner. 2021. Innate cell microenvironments in lymph nodes shape the generation of T cell responses during type I inflammation. *Sci. Immunol.* 6: eabb9435.
22. Heil, M., and W. G. Land. 2014. Danger signals – damaged-self recognition across the tree of life. *Front Plant Sci* 5: 578.
23. Di Virgilio, F., D. Dal Ben, A. C. Sarti, A. L. Giuliani, and S. Falzoni. 2017. The P2X7 receptor in infection and inflammation. *Immunity* 47: 15–31.
24. Borges da Silva, H., L. K. Beura, H. Wang, E. A. Hanse, R. Gore, M. C. Scott, D. A. Walsh, K. E. Block, R. Fonseca, Y. Yan, et al. 2018. The purinergic receptor P2RX7 directs metabolic fitness of long-lived memory CD8$^+$ T cells. *Nature* 559: 264–268.
25. Borges da Silva, H., C. Peng, H. Wang, K. M. Wanhainen, C. Ma, S. Lopez, A. Khoruts, N. Zhang, and S. C. Jameson. 2020. Sensing of ATP via the purinergic receptor P2RX7 promotes CD8$^+$ Trm cell generation by enhancing their sensitivity to the cytokine TGF-β. *Immunity* 53: 158–171.e6.
26. Zhang, N., and M. J. Bevan. 2013. Transforming growth factor-β signaling controls the formation and maintenance of gut-resident memory T cells by regulating migration and retention. *Immunity* 39: 687–696.
27. Skon, C. N., J. Y. Lee, K. G. Anderson, D. Masopust, K. A. Hogquist, and S. C. Jameson. 2013. Transcriptional downregulation of S1pr1 is required for the establishment of resident memory CD8$^+$ T cells. *Nat. Immunol.* 14: 1285–1293.
28. Steinert, E. M., J. M. Schenkel, K. A. Fraser, L. K. Beura, L. S. Manlove, B. Z. Igyártó, P. J. Southern, and D. Masopust. 2015. Quantifying memory CD8 T cells reveals regionalization of immunosurveillance. *Cell* 161: 737–749.
29. Borges da Silva, H., H. Wang, L. J. Qian, K. A. Hogquist, and S. C. Jameson. 2019. ARTC2.2/P2RX7 signaling during cell isolation distorts function and quantification of tissue-resident CD8$^+$ T cell and invariant NKT subsets. *J. Immunol.* 202: 2153–2163.
30. Renkema, K. R., J. Y. Lee, Y. J. Lee, S. E. Hamilton, K. A. Hogquist, and S. C. Jameson. 2016. IL-4 sensitivity shapes the peripheral CD8$^+$ T cell pool and response to infection. *J. Exp. Med.* 213: 1319–1329.
31. Anderson, K. G., K. Mayer-Barber, H. Sung, L. Beura, B. R. James, J. J. Taylor, L. Qunaj, T. S. Griffith, V. Vezys, D. L. Barber, and D. Masopust. 2014. Intravascular staining for discrimination of vascular and tissue leukocytes. *Nat. Protoc.* 9: 209–222.
32. Love, M. I., W. Huber, and S. Anders. 2014. Moderated estimation of fold change and dispersion for RNA-seq data with DESeq2. *Genome Biol.* 15: 550.
33. Seki, A., and S. Rutz. 2018. Optimized RNP transfection for highly efficient CRISPR/Cas9-mediated gene knockout in primary T cells. *J. Exp. Med.* 215: 985–997.
34. Graef, P., V. R. Buchholz, C. Stemberger, M. Flossdorf, L. Henkel, M. Schiemann, I. Drexler, T. Höfer, S. R. Riddell, and D. H. Busch. 2014. Serial transfer of single-cell-derived immunocompetence reveals stemness of CD8$^+$ central memory T cells. *Immunity* 41: 116–126.
35. Masopust, D., D. Choo, V. Vezys, E. J. Wherry, J. Duraiswamy, R. Akondy, J. Wang, K. A. Casey, D. L. Barber, K. S. Kawamura, et al. 2010. Dynamic T cell migration program provides resident memory within intestinal epithelium. *J. Exp. Med.* 207: 553–564.
36. Renkema, K. R., M. A. Huggins, H. Borges da Silva, T. P. Knutson, C. M. Henzler, and S. E. Hamilton. 2020. KLRG1$^+$ memory CD8 T cells combine properties of short-lived effectors and long-lived memory. *J. Immunol.* 205: 1059–1069.
37. Mackay, L. K., A. Rahimpour, J. Z. Ma, N. Collins, A. T. Stock, M. L. Hafon, J. Vega-Ramos, P. Lauzurica, S. N. Mueller, T. Stefanovic, et al. 2013. The developmental pathway for CD103$^+$CD8$^+$ tissue-resident memory T cells of skin. *Nat. Immunol.* 14: 1294–1301.
38. Kalia, V., S. Sarkar, S. Subramaniam, W. N. Haining, K. A. Smith, and R. Ahmed. 2010. Prolonged interleukin-2Rα expression on virus-specific CD8$^+$ T cells favors terminal-effector differentiation in vivo. *Immunity* 32: 91–103.

39. Dominguez, C. X., R. A. Amezquita, T. Guan, H. D. Marshall, N. S. Joshi, S. H. Kleinstein, and S. M. Kaech. 2015. The transcription factors ZEB2 and T-bet cooperate to program cytotoxic T cell terminal differentiation in response to LCMV viral infection. *J. Exp. Med.* 212: 2041–2056.
40. Guan, T., C. X. Dominguez, R. A. Amezquita, B. J. Laidlaw, J. Cheng, J. Henao-Mejia, A. Williams, R. A. Flavell, J. Lu, and S. M. Kaech. 2018. ZEB1, ZEB2, and the miR-200 family form a counterregulatory network to regulate $CD8^+$ T cell fates. *J. Exp. Med.* 215: 1153–1168.
41. Omilusik, K. D., J. A. Best, B. Yu, S. Goossens, A. Weidemann, J. V. Nguyen, E. Seuntjens, A. Stryjewska, C. Zweier, R. Roychoudhuri, et al. 2015. Transcriptional repressor ZEB2 promotes terminal differentiation of $CD8^+$ effector and memory T cell populations during infection. *J. Exp. Med.* 212: 2027–2039.
42. Viola, A., R. L. Contento, and B. Molon. 2006. T cells and their partners: the chemokine dating agency. *Trends Immunol.* 27: 421–427.
43. Wanhainen, K. M., S. C. Jameson, and H. B. da Silva. 2019. Self-regulation of memory CD8 T cell metabolism through extracellular ATP signaling. *Immunometabolism* 1: e190009.
44. Woehrle, T., L. Yip, A. Elkhal, Y. Sumi, Y. Chen, Y. Yao, P. A. Insel, and W. G. Junger. 2010. Pannexin-1 hemichannel-mediated ATP release together with P2X1 and P2X4 receptors regulate T-cell activation at the immune synapse. *Blood* 116: 3475–3484.
45. Stark, R., T. H. Wesselink, F. M. Behr, N. A. M. Kragten, R. Arens, F. Koch-Nolte, K. P. J. M. van Gisbergen, and R. A. W. van Lier. 2018. T_{RM} maintenance is regulated by tissue damage via P2RX7. *Sci. Immunol.* 3: eaau1022.
46. Dudek, M., D. Pfister, S. Donakonda, P. Filpe, A. Schneider, M. Laschinger, D. Hartmann, N. Hüser, P. Meiser, F. Bayerl, et al. 2021. Auto-aggressive $CXCR6^+$ CD8 T cells cause liver immune pathology in NASH. [Published erratum appears in 2021 *Nature* 593: E14.] *Nature* 592: 444–449.
47. Jadhav, R. R., S. J. Im, B. Hu, M. Hashimoto, P. Li, J. X. Lin, W. J. Leonard, W. J. Greenleaf, R. Ahmed, and J. J. Goronzy. 2019. Epigenetic signature of $PD\text{-}1^+$ $TCF1^+$ CD8 T cells that act as resource cells during chronic viral infection and respond to PD-1 blockade. *Proc. Natl. Acad. Sci. USA* 116: 14113–14118.
48. Chang, J. T., V. R. Palanivel, I. Kinjyo, F. Schambach, A. M. Intlekofer, A. Banerjee, S. A. Longworth, K. E. Vinup, P. Mrass, J. Oliaro, et al. 2007. Asymmetric T lymphocyte division in the initiation of adaptive immune responses. *Science* 315: 1687–1691.
49. Chang, J. T., M. L. Ciocca, I. Kinjyo, V. R. Palanivel, C. E. McClurkin, C. S. Dejong, E. C. Mooney, J. S. Kim, N. C. Steinel, J. Oliaro, et al. 2011. Asymmetric proteasome segregation as a mechanism for unequal partitioning of the transcription factor T-bet during T lymphocyte division. *Immunity* 34: 492–504.
50. Arsenio, J., B. Kakaradov, P. J. Metz, S. H. Kim, G. W. Yeo, and J. T. Chang. 2014. Early specification of $CD8^+$ T lymphocyte fates during adaptive immunity revealed by single-cell gene-expression analyses. *Nat. Immunol.* 15: 365–372.
51. Oliaro, J., V. Van Ham, F. Sacirbegovic, A. Pasam, Z. Bomzon, K. Pham, M. J. Ludford-Menting, N. J. Waterhouse, M. Bots, E. D. Hawkins, et al. 2010. Asymmetric cell division of T cells upon antigen presentation uses multiple conserved mechanisms. *J. Immunol.* 185: 367–375.
52. Lin, W. H., W. C. Adams, S. A. Nish, Y. H. Chen, B. Yen, N. J. Rothman, R. Kratchmarov, T. Okada, U. Klein, and S. L. Reiner. 2015. Asymmetric PI3K signaling driving developmental and regenerative cell fate bifurcation. *Cell Rep.* 13: 2203–2218.
53. Youngblood, B., J. S. Hale, H. T. Kissick, E. Ahn, X. Xu, A. Wieland, K. Araki, E. E. West, H. E. Ghoneim, Y. Fan, et al. 2017. Effector CD8 T cells dedifferentiate into long-lived memory cells. *Nature* 552: 404–409.
54. Akondy, R. S., M. Fitch, S. Edupuganti, S. Yang, H. T. Kissick, K. W. Li, B. A. Youngblood, H. A. Abdelsamed, D. J. McGuire, K. W. Cohen, et al. 2017. Origin and differentiation of human memory CD8 T cells after vaccination. *Nature* 552: 362–367.
55. Herndler-Brandstetter, D., H. Ishigame, R. Shinnakasu, V. Plajer, C. Stecher, J. Zhao, M. Lietzenmayer, L. Kroehling, A. Takumi, K. Kometani, et al. 2018. $KLRG1^+$ effector $CD8^+$ T cells lose KLRG1, differentiate into all memory T cell lineages, and convey enhanced protective immunity. *Immunity* 48: 716–729.e8.
56. Tay, R. E., O. Olawoyin, P. Cejas, Y. Xie, C. A. Meyer, Y. Ito, Q. Y. Weng, D. E. Fisher, H. W. Long, M. Brown, et al. 2020. Hdac3 is an epigenetic inhibitor of the cytotoxicity program in CD8 T cells. [Published erratum appears in 2020 *J. Exp. Med.* 217: e2019145305152020c.] *J. Exp. Med.* 217: e20191453.
57. Carty, S. A., M. Gohil, L. B. Banks, R. M. Cotton, M. E. Johnson, E. Stelekati, A. D. Wells, E. J. Wherry, G. A. Koretzky, and M. S. Jordan. 2018. The loss of TET2 promotes $CD8^+$ T cell memory differentiation. *J. Immunol.* 200: 82–91.
58. Gullicksrud, J. A., F. Li, S. Xing, Z. Zeng, W. Peng, V. P. Badovinac, J. T. Harty, and H. H. Xue. 2017. Differential requirements for Tcf1 long isoforms in $CD8^+$ and $CD4^+$ T cell responses to acute viral infection. *J. Immunol.* 199: 911–919.
59. Hashimoto-Hill, S., L. Friesen, M. Kim, and C. H. Kim. 2017. Contraction of intestinal effector T cells by retinoic acid-induced purinergic receptor P2X7. *Mucosal Immunol.* 10: 912–923.
60. Kurd, N. S., Z. He, T. L. Louis, J. J. Milner, K. D. Omilusik, W. Jin, M. S. Tsai, C. E. Widjaja, J. N. Kanbar, J. G. Olvera, et al. 2020. Early precursors and molecular determinants of tissue-resident memory $CD8^+$ T lymphocytes revealed by single-cell RNA sequencing. *Sci. Immunol.* 5: eaaz6894.
61. Kok, L., F. E. Dijkgraaf, J. Urbanus, K. Bresser, D. W. Vredevoogd, R. F. Cardoso, L. Perié, J. B. Beltman, and T. N. Schumacher. 2020. A committed tissue-resident memory T cell precursor within the circulating $CD8^+$ effector T cell pool. *J. Exp. Med.* 217: e20191711.